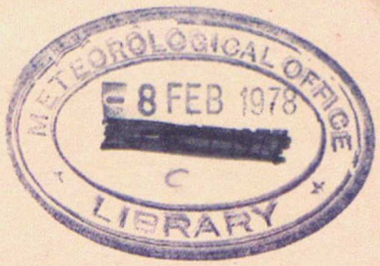

METEOROLOGICAL OFFICE
RADAR RESEARCH
LABORATORY

RSRE MALVERN ENGLAND

RESEARCH REPORT

October 1977, No.4

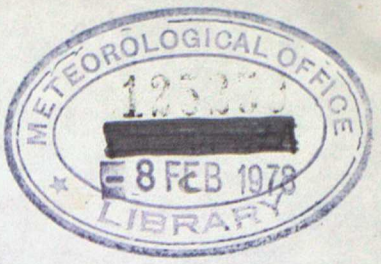

METEOROLOGICAL APPLICATIONS OF RADAR

K A Browning

Meteorological Office Radar Research Laboratory

Royal Signals and Radar Establishment

Malvern

ABSTRACT

Radar has been used by meteorologists for 30 years or so but it is only during the latter half of this period that the full measure of its versatility has come to be recognised. Operationally important techniques have been or are being developed to identify and track severe storms, to provide warning of tornadoes, to measure and forecast rainfall quantitatively, and to measure winds, turbulence and wind shear. At the same time research meteorologists are using specialised radar techniques to investigate many poorly understood aspects of atmospheric behaviour: to identify the physics of clear air turbulence, the dynamics of fronts, the structure of the atmospheric boundary layer, the 3-dimensional airflow and trajectories of hailstones in thunderstorms, and the patterns of precipitation within mid-latitude depressions. Studies such as these are giving fresh impetus to a branch of meteorology, mesoscale meteorology, which largely because of the difficulty of obtaining definitive observations has hitherto been a neglected field. This article highlights the strengths and limitations of radar as a tool for observing the atmosphere and attempts to provide a balanced view of its many applications in meteorology.

CONTENTS

1 INTRODUCTION

The physical mechanisms occurring in the atmosphere are of many kinds and span a wide range of scales. At the lower end of the spectrum of scales are microscale phenomena such as those associated with individual cloud and precipitation particles and with turbulent flows. These topics have been amenable to laboratory and field experimentation often using quite simple in situ instruments and their physics is correspondingly well established. At the other end of the spectrum there are wavelike atmospheric disturbances with characteristic dimensions larger than 1000 km which dictate the broad nature of the weather on time scales of a week or more. These macroscale phenomena can be observed quite well by means of data from the worldwide network of radiosonde stations and , more recently, satellites. Thus, although some deficiencies in observational capability remain, good progress has been made in the understanding of the larger scales, too. Where progress has been slowest is with the intermediate-scale phenomena with horizontal dimensions from kilometres to many hundreds of kilometres. This range covers what meteorologists call the mesoscale. A lot of our weather occurs on the mesoscale : consider, for example, the clear air turbulence that causes discomfort to air passengers near jet streams, the rare occurences of strong wind shear that can affect an aircraft during landing and take-off, and the torrential downpours with hail and tornadoes that can be produced by severe thunderstorms; or consider the local outbreaks of heavy rain associated with convective cells embedded within widespread frontal rain, the sea breezes that occasionally trigger showers near coasts, and the arrays of thermals and lee waves sought out by glider pilots - all of these phenomena are organised on the mesoscale.

Mesoscale phenomena are important in themselves and, sometimes, because of their interaction with other scales. The mesoscale dynamics of convective clouds, for example, needs to be understood if its bulk

effect is to be properly parameterised when modelling the macroscale behaviour of the atmosphere for long range forecasting and studies of climatic change. The mesoscale motions within clouds also determine the environmental factors that control the microphysical processes of precipitation growth and these need to be better understood if further progress is to be made in the controversial areas of precipitation enhancement and hail suppression.

Part of the reason for the slow progress in acquiring an understanding of mesoscale phenomena lies in their complex and transient nature. But just as important is the fact, stressed by Orlanski (1975), that mesoscale phenomena are very difficult to observe. They fall between two stools in the sense that they are too big to be embraced by a single observer equipped with direct sensing equipment yet small enough to be lost between networks of conventional upper air observations. This is where radar comes into its own as a meteorological tool, for a single radar - as we shall show in this review - has the capacity for remotely probing the structure of a remarkable variety of phenomena, three-dimensionally and almost instantaneously, in all directions out to ranges of order 100 km. Indeed it is probably fair to say that radar has made a broader contribution than any other single tool to the surge of activity in the field of meso-meteorology which has been gathering momentum during the last decade or so.

The purpose of this article is to provide an overview of the varied applications of radar in meteorology. In an article of this length we must necessarily be selective. We shall concentrate on bringing out the essential strengths and limitations of radar - both fundamental and practical. Highly technical matters are avoided where possible and no attempt is made to achieve an exhaustive bibliography. These can be found in text books:

for example, Skolnik (1962) provides an introduction to radar systems, while Battan (1973) provides an account of the range of radar techniques available for observing the atmosphere. Our aim, rather, is to appeal to the physicist or meteorologist with a general interest in the atmosphere but lacking specialised knowledge of radar or mesoscale meteorology. We attempt throughout to put radar in its appropriate place within the wider meteorological context, adopting the point of view of the potential user. We are careful to indicate the stage of development of the various techniques described. Some of the techniques discussed in Secs 3, 4 and 5, for example, are already being used operationally; others, especially those discussed in Secs 6 and 7, are restricted to a small research community.

Only ground-based microwave radars are considered in this review. We also restrict ourselves to monostatic techniques. Bistatic radars, employing widely separated transmitters and receivers, are excluded; so too are acoustic radar (sodar) and laser radar (lidar).

2 BROAD CATEGORIES OF RADAR TECHNIQUE AVAILABLE TO THE METEOROLOGIST

For radar to provide useful meteorological information it is necessary to have some kind of airborne target. Sometimes man-made targets are used. It is well known, for example, that special reflectors are often attached to balloon-borne radiosondes and these are tracked by radar to obtain winds. A limitation of this method, which is used routinely at many upper air stations, is that each balloon provides only a single wind profile. Thus this method is not well-suited to defining mesoscale fields of air motion. Dropsondes released from aircraft are easier to dispense in great numbers as an areal array and this appears to be a promising technique if their position is derived from one of the world-wide systems of radio navigation beacons (Ryder, unpublished). But, if the dropsondes are tracked by radar (eg Hardman et al 1972), there is still a severe limitation on the number of wind soundings that can be obtained in a given time. Strips of metal foil tuned to the radar wavelength, called chaff, may also be released and these can be very useful as tracers of the airflow in special circumstances (eg Marwitz 1973, Hildebrand 1975). However, the versatility of radar is most evident when the meteorologist uses radar to detect natural targets and this will be the main topic of this review. The kind of targets of greatest interest are precipitation (rain, snow and hail), refractive index inhomogeneities (associated with small irregularities of humidity and temperature) and even small insects (which drift with the wind and trace the air motion). Radar echoes from natural targets are ubiquitous and are often regarded by air traffic controllers as a nuisance; they are referred to as weather 'clutter'. But to the meteorologist these echoes convey valuable information both about the targets themselves and about the meso-scale fields of air motion associated with them.

The meteorologist is interested in four aspects of the radar echo from an assemblage of natural targets:

(i) its intensity, or reflectivity,

(ii) its shape

(iii) its location as a function of time, and

(iv) its Doppler frequency spectrum.

We have subdivided this review as far as possible according to these four categories. In Sec 3 we consider the intensity of the radar echo as a means of measuring precipitation quantitatively. In Sec 4 we consider the shape of radar echoes from precipitation as a means of inferring the type of dynamical system responsible for generating that precipitation. In Sec 5 we show how modern digital techniques of handling data on the location and movement of precipitation areas permit radar to be exploited for short period forecasting of precipitation. In Sec 6, we show how the measurement of the Doppler shift of the energy backscattered from precipitation is being used by research meteorologists to provide information about the nature of the precipitation particles and the associated fields of air motion and turbulence. Then, in Sec 7, all of these radar techniques are reconsidered, but with radars of high sensitivity in mind which are capable of detecting abundant echoes from clear air targets as well as from precipitation.

3 QUANTITATIVE MEASUREMENT OF PRECIPITATION

3.1 Measurement of rainfall intensity

The quantitative measurement of rainfall is of great practical importance. The traditional rainguage provides a fairly accurate method of obtaining measurements at a point but there is a greater requirement by meteorologists, hydrologists, communications engineers and others for detailed measurements of the mesoscale pattern of rainfall over extended areas. Often these measurements are needed in real time. It is likely that radar techniques will become the standard method of meeting many of these requirements, partly because of the unique capability of radar to observe the areal

distribution of precipitation and partly because data from a large area are immediately available at a single centre with a minimum of telemetry requirements. When the subject was reviewed by Harrold (1965), World Meteorological Organization (1966) and Kessler (1968), there were still some practical problems in the way of the operational use of quantitative radar techniques. It is only during the last decade that progress in data processing and communications, together with experimental assessments of accuracy, have confirmed the practical utility of radar in this field.

Techniques of measuring rainfall by radar fall into two broad categories. One depends on a relationship between rainfall rate R and the associated attenuation of the radar energy; the other depends on a relationship between R and the intensity of the backscattered radiation, or radar reflectivity. A third, more sophisticated method, which we shall mention only in passing, combines measurements of attenuation and reflectivity made simultaneously at two wavelengths. This approach has been suggested by Abshaev (1971), Eccles and Mueller (1971) and Atlas and Ulbrich (1974) as a way of measuring not only R but also liquid water content and the median volume diameter of the raindrops.

The simple attenuation method of measuring rainfall exploits the fact that the microwave attenuation by rainfall at wavelengths near 1 cm is related nearly linearly to the rainfall rate (Ryde 1947, Wexler and Atlas 1963), this being the case regardless of variations in the drop size distribution of the rain (Atlas and Ulbrich 1976). The linear relationship formed the basis of several experiments to measure path-integrated rainfall at a wavelength of 8.6 mm using two or more known targets along a path (eg Collis and Ligda 1961, Harrold 1967). The difficulties with this technique are the need for large numbers of remote targets (or receivers) to achieve areal measurements and occasionally the total loss of signal owing to excessive attenuation in heavy rain. Thus, although this method is potentially useful

for path-integrated measurements in non-torrential rain, the approach which has been generally adopted as the basic radar-rainfall technique exploits instead the relationship between rainfall rate and radar reflectivity. Because of its practical importance, we now consider this latter approach in some detail.

The radar reflectivity approach of measuring rainfall involves the measurement of the radar energy (P) scattered back to the radar aerial by the raindrops within a number of pulse volumes, each one defined as in Fig 1 by the radar beamwidth (θ) the range (r) and the pulse length (l). Measurements are made simultaneously in pulse volumes at many ranges out to 100 km or more and typically at different azimuths as the beam rotates about a vertical axis. Probert-Jones (1962) has shown that, provided the pulse volume is uniformly filled by rain, then

$$\overline{P}_r = C_1 C_2 K \frac{Z}{r^2} \qquad (1)$$

where $\overline{P}_r$ is the average power returned from the rain at range r, C_1 is a function of the known radar parameters, C_2 is approximately a constant related to the dielectric properties of the raindrops, K is the coefficient of attenuation (due mainly to rain) as the radiation traverses to and from the range of interest, and Z is the radar reflectivity factor, defined as the summation per unit volume of the sixth power of the drop diameters. The simple sixth-power relationship is a direct consequence of the Rayleigh scattering law which applies as long as the radar wavelength is long compared with the diameter of the scattering particles. This is not valid for radar scattering from large hail (Sec 3.5), but it does hold good for rain at the wavelengths normally used in weather radars (Sec 3.2.5).

The reflectivity factor Z in eq (1) is related to the rainfall rate through the equation:

$$Z = aR^b \qquad (2)$$

where R is the rainfall rate and a and b are empirical constants. While the measurement of rainfall outlined above is straightforward in concept, there are a number of difficulties which call for careful experimental design. In addition to some natural variability in the 'constants' a and b in eq (2), there are problems arising from the fluctuating character of the radar echo from rain and from the fact, illustrated in Fig 1, that the pulse volume at long ranges is a considerable distance above the ground. These and related problems are considered next.

3.2 Practical considerations in the measurement of surface rainfall

3.2.1 Signal fluctuations from rain

The radar signal from rain is the sum of the signals from all the raindrops distributed and moving at random in each pulse volume. The result is a strongly fluctuating signal for which the average power, $\overline{P}_r$, contains information about the rainfall intensity while the fluctuations contain information about the radial motion of the raindrops. The fluctuations provide the basis of a ground clutter discrimination method described later; however, the very existence of such fluctuations means that the average must be obtained with some care.

The theory of fluctuating echoes from randomly distributed particles was developed by Marshall and Hitschfeld (1953) and Wallace (1953). They showed that for a set of independent samples of the back-scattered power, P_r, the probability of P_r falling between values of P_r and $P_r + dP_r$ is given by $\frac{1}{\overline{P}_r} e^{-P_r/\overline{P}_r} dP_r$. Marshall and Hitschfeld derived the number of independent pulses, k, that needs to be integrated in order to keep errors of $\overline{P}_r$ within certain limits. They found, for example, that if k = 25, the measured $\overline{P}_r$ would be within $\pm$ 40% of the correct value 95% of the time. This accuracy is comparable to that generally achieved in the experimental measurement of echo power and so there is little point in integrating many more than 25 independent pulses (Atlas 1964).

Integration can be carried out over samples of P_r that are separated in range or time (or both). In the case of range integration, the averaging is carried out over adjacent pulse volumes. In the case of time integration, the interval between independent samples depends on the fluctuating characteristics of the array of raindrops and on the radar wavelength. For a typical situation a period of order 10 ms is required for the raindrops to shuffle from one array to another independent one (Lhermitte 1963). In this case not every pulse emitted by a radar with a pulse repetition frequency (PRF) of 300 s^{-1} would be independent. If integration in time is to be achieved for a radar scanning in azimuth without degrading azimuth resolution, then the required number of independent samples must be received before the aerial rotates through a beamwidth. This places a limitation on the maximum permissable rotation rate. The need for appropriate integration is well understood, however, and errors arising from inadequate integration are usually small compared with some of the other sources of error described next.

3.2.2 Variability of drop-size distribution

Since the reflectivity factor Z depends on the sixth power of the drop diameter, the Z-R relationship, unlike the attenuation-rainfall relationship, depends sensitively on the nature of the rain drop size distribution. There have been many studies of the Z-R relation (see Stout and Mueller (1968) and Battan (1973) for summaries) and there are, unfortunately, almost as many Z-R relationships as there are studies. Thus it has been common practice in the past to use a 'standard' relationship, $Z = 200\ R^{1.6}$, based on the results of Marshall and Palmer (1948). By taking into account the character of the precipitation system, it may be possible to do better than this. Joss et al (1970), for example, found that the constant 'a' in the Z-R relation varied from 140 for drizzle, through 250 for widespread rain, to 500 for thunderstorm rain, and he suggested that it might be possible to

use automatic computer methods of identifying the character of the precipitation echo to select the most appropriate Z-R relation. The fact remains, however, that the spatial and temporal variability of drop size distribution is so great that in practice the best approach is to use a number of raingauges to calibrate the radar (Wilson 1970 and 1975, Harrold et al 1974). The use of this "ground truth" calibration approach is fundamental to the proper use of radar. Not only does it allow for variations in drop size distribution but it also takes into account any changes in performance of the radar system. It takes into account, too, the changes in reflectivity with height which are discussed next.

3.2.3 Problems arising from the variation of reflectivity in the vertical

The curvature of the earth causes the radar beam to rise a considerable distance above the surface at long ranges (Fig 1). For example, even if the radar horizon were at 0 deg, the bottom of the beam would be at a height (h) of almost 1 km at a range of 100 km, while at 200 km it would be over 2 km. This leads to three difficulties in the measurement of surface rainfall intensity:

One problem is the non-vertical orientation of precipitation shafts owing to wind shear. This may be quite troublesome in the case of slow-falling snow particles (Sec 3.4) and, according to Harrold et al (1974), is not altogether negligible even for raindrops falling at several metres per second, especially when detailed rainfall mapping is required (eg over small urban catchments). In these cases rough corrections can be applied using conventionally available wind information.

Another problem caused by measuring reflectivity aloft rather than at the surface is that it fails to take into account growth or evaporation of rain at low levels. According to Harper (1957) there is often very little low-level growth or evaporation in widespread rain over uniform terrain. There are nevertheless occasions, for example ahead of warm fronts

(Harrold 1973) and occlusions (Houze et al 1976), when an elevated layer of precipitation evaporates either partially or entirely within dry air in the lowest 2 or 3 kilometres. In hilly region, especially on windward-slopes when the low-level flow is saturated and the winds are strong (Nash and Browning 1978), substantial growth may occur at low levels. To some extent this low-level growth can be allowed for by applying climatological correction factors. In principle low-level growth can also be calculated from a sufficiently detailed knowledge of the meteorological situation (Bader and Roach 1977). These correction procedures are of limited accuracy, however, and so where possible the low-level precipitation should be observed directly by using a low elevation angle and by restricting the range to which quantitative measurements are attempted.

A third problem caused by the elevation of the radar beam is the increased likelihood of the beam intercepting sleet in the melting layer. The average height of the melting layer over England in winter is about 1 km (Collier 1976). As discussed by Battan (1973), the reflectivity factor in the melting layer in situations of widespread rain may be enhanced by a factor of 10 compared with that in the precipitation above and below it, mainly because of changes in dielectric constant and fallspeed, and aggregation of wet snowflakes. Accordingly the sleet layer is seen by radar as an intense band of echo. Although this provides the basis of a method of measuring the height of the melting level, it serves to confuse the interpretation of rainfall intensity. Schemes have been devised to correct for the interception of the so-called bright band (eg Harrold et al 1974, Harrold and Kitchingman 1975) but these are only partial solutions and have yet to be fully tested. Use of a calibration raingauge in an area contaminated by interception of the bright band is the best solution where such a gauge exists. In general it is important to minimise the number of occasions when the bright band is intersected by using a narrow beam at the lowest possible elevation angle.

3.2.4 The effects of screening and ground clutter

The previous discussion emphasises the need to keep the radar beam low. By doing this, however, a fresh set of problems is incurred because, in the case of a radar sited amidst irregular terrain with the beam directed almost horizontally, some or all of the beam will be intercepted by hills at various ranges. Although one attempts to minimise these difficulties by locating the radar at an unobstructed site, these difficulties can never be avoided altogether. There are two problems. First, there is screening of the main beam such that only a fraction of the power illuminates the rain at the longer ranges. This can be corrected for provided at least 60% of the beam is unobstructed (Harrold et al 1974). Secondly, there are echoes from the ground, known as permanent echoes or ground clutter, which may obscure the wanted returns from the rain. This problem exists even when there are no obstructions within the main beam because small amounts of energy transmitted within the sidelobes of the aerial radiation pattern still produce detectable echoes from certain targets particularly in urban areas.

The problem of ground clutter can be tacked in three ways. The first is for data at close ranges, where most of the ground echoes occur, to be acquired with the beam elevated to prevent the main lobe intersecting the ground. For the reasons given above, data at long ranges must be acquired at the lowest possible elevation angle. Thus the best field of surface rainfall is obtained by combining data from aerial rotations made at two (or possibly more) elevation angles. It is not possible to avoid ground clutter entirely in this way without compromising the need to collect data at low altitudes, and so other techniques are required as well. A second very simple technique is to store a map of known ground clutter locations, to discard the radar measurements in such areas and, provided these areas are not too large, to interpolate across them on the basis of surrounding

uncontaminated radar data. The third countermeasure, which although very promising has yet to be tested fully in an operational environment, exploits the different characteristics of the signal fluctuations from ground clutter and precipication.

Nathanson (1969) has shown that for a typical radar beam width of 1.5 deg the rms bandwidth of signal from precipitation varies from 1 m s^{-1} at a range of about 20 km to 4 m s^{-1} at about 90 km. On the other hand, the bandwidth of ground return from a woodland area, say, varies from only 0.025 m s^{-1} in the presence of a wind speed of 2 m s^{-1} to about 0.5 m s^{-1} at a wind speed of 30 m s^{-1}. Thus, as Johnson et al (1975) points out, the fluctuation rate of the radar return should be useful in discriminating precipitation echoes from ground clutter. To achieve this discrimination it is necessary to avoid introducing spurious fluctuations owing to an unstable transmitter or too fast an aerial rotation rate. One of the attractions of this technique is that it can be used to discriminate against the more widespread ground clutter that occasionally occurs as a result of anomalous refraction of the radar beam. This situation, known as anomalous propagation or 'anaprop', occurs when there is a shallow layer of relatively cool and/or moist air with low refractive index close to the ground capped by a layer of much higher refractive index, and it is particularly common in certain geographical areas (Bean and Dutton 1968). In most parts of Britain anomalous propagation is uncommon in the presence of widespread rain; however, it occurs sometimes in association with the cold outflows from thunderstorms and in some fair weather situations.

3.2.5 Choice of radar wavelength : a compromise between attenuation and beamwidth

One of the factors that impeded the early application of radar for measuring rainfall quantitatively was the common use of radars operating at a wavelength of 3 cm (Austin 1964). Radiation at this wavelength suffers

considerable attenuation in passing through liquid precipitation; for example, there is a 1-way loss of almost 0.1 dB per km in the presence of a rainfall rate of 4 mm hr^{-1} (eg Skolnik 1962). Whilst this attenuation can serve as the basis for path-integrated rainfall measurements between the radar and known targets (Sec 3.1), it is a major source of error in the absolute measurement of reflectivity. It is possible in principle to correct for this attenuation using the radar data itself to infer the precipitation intensity and hence the attenuation; however, the errors are cumulative in range, and Hitschfeld and Bordan (1954) have shown that in practice such corrections cannot be applied with any success. As meteorologists became fully aware of this situation, there was a swing towards the use of radars operating at a wavelength of 10 cm for which attenuation by rain is negligible. (Attenuation by oxygen is not entirely negligible but it is small enough to be easily corrected for). The use of a wavelength of 10 cm is a wise choice for tropical areas subject to frequent torrential rain, but other considerations suggest that a shorter wavelength is more appropriate for use in temperate regions:

For an aerial of given size, and hence cost, the beamwidth is inversely proportional to wavelength. We have already seen that the beam needs to be narrow to be able to measure rain at the lowest possible altitude without encountering the ground. Thus for radars in temperate parts of the world, it is most cost-effective to use a wavelength intermediate between 3 cm (the so-called X-Band) and 10 cm (S-Band). A suitable wavelength available for meteorological use is 5.6 cm (C-Band). At this wavelength the attenuation, although significant, is small enough to be accurately allowed for (Weible and Sirmans 1976).

3.3 Accuracy of surface rainfall measurements using radar calibrated against raingauges

There have been many studies of the accuracy of rainfall measurements

by radar (see review by Harrold and Nicholass 1972). Recent studies in which radar has been calibrated against raingauges (Wilson 1970 and 1975, Harrold et al 1974, Woodley et al 1975) have shown that the accuracy of areal rainfall measurements depends on the density and proximity of the calibration gauges, the period of measurement, the amount of rainfall, and the size of the area and its proximity to the radar. At a range of 200 km radar generally provides only a qualitative means of detecting an area of rain. Indeed, since the radar beam is likely to be far above the ground, the radar may fail altogether to detect precipitation from shallow systems at such ranges. For a well-sited radar the rapid deterioration in accuracy sets in at about 100 km range and, in round figures, this can be considered to be the limit of quantitative rainfall measurements.

Most studies of measurement accuracy have been carried out over flat terrain, often with an emphasis on showery rain. For hydrological purposes it is important to measure areal rainfall over hill catchments, and for widespread as well as showery rain. A comprehensive set of such measurements has recently been completed as part of the Dee Weather Radar Project (DWRP) (Collier 1977) and we shall discuss the results of this experiment in some detail :

The accuracy with which a 10 cm radar with a 2 deg conical beamwidth and also a 5.6 cm radar with a 1 deg beam were able to measure areal rainfall in a hilly region of North Wales was assessed in the DWRP by comparison with a dense network of 76 autographic raingauges distributed over an area of almost 1000 km^2. The main experimental area was within 50 km of the radar. Assessment of the accuracy of radar is not an easy task, because the standard of comparison is itself subject to significant errors, not the least of which are those arising from the unrepresentativeness of individual gauges. For this reason the accuracy of the radar, calibrated using a specified small number of gauges, was assessed against a so-called optimum

rainfall field. The optimum rainfall field was derived from the entire field of 76 gauges assuming that each gauge measured the rainfall accurately at its location (unless comparison with its nearest neighbours indicated a gross error) but using the pattern of radar reflectivity to interpolate between the gauges to obtain the best possible definition of features on a scale smaller than the gauge spacing. The advantages gained in this way were considered to outweigh the element of bias introduced into the assessment.

The DWRP was designed with the hydrological user in mind and, since he requires integrated values of rainfall, accuracy was assessed in terms of hourly totals integrated over individual river sub-catchments with areas of typically 60 km^2. On occasions when the beam did not intersect the melting level, the radar estimates of hourly rainfall over the subcatchments were found to differ from the optimum estimate by about 15% within 15 km of a calibration gauge and 20% at distances of about 20 km from a calibration gauge. When the melting level was encountered these errors increased on average by a factor of about 1.5. Fig 2 shows how the accuracy of the radar estimates of rainfall increased as both the averaging period and the averaging area increased. For areas in excess of about 450 km^2, however, the accuracy began to drop again because the calibration gauge became unrepresentative of the larger area.

It is interesting to compare the accuracy of radar with that achievable with raingauge networks of different densities. The solid curves in Fig 3 represent the accuracy of hourly rainfall totals over subcatchments that can be achieved with a calibrated radar located within 50 km of the area of interest. The dotted curves represent the accuracy achieved with networks of raingauges in the absence of radar. For both sets of curves accuracy is plotted as a function of raingauge density. The accuracy of the raingauge networks depends critically on the nature of the rain, as shown

by the large differences in the four dotted curves. The radar measurements, on the other hand, were nearly independent of rainfall type. It can be seen, for example, that the radar system calibrated using 2 raingauges over the 1000 km^2 experimental area had the same accuracy as a raingauge network of 9 gauges per 1000 km^2 in the presence of typical widespread rain. In showery situations, the same radar system had an accuracy comparable with a raingauge network with a density of about 50 gauges per 1000 km^2. The above results apply when the radar beam does not intersect the melting level; Fig 3 shows that when it does the mean error of the radar estimates increases from 20% to 30%, again assuming 2 calibrating gauges per 1000 km^2. Although the main assessment of accuracy in the DWRP was carried out over a limited azimuth sector with an area of only 1000 km^2, the area covered quantitatively by such a radar is more than an order of magnitude greater. If accurate measurements of rainfall are required over large areas it becomes increasingly impractical to use raingauges alone, especially when the gauges have to be telemetered to provide data in real time. It has been estimated (Water Resources Board 1973) that, if an accuracy of 25% is required, the cost-effectiveness of a calibrated radar system exceeds that of a telemetering raingauge network provided measurements are required over an area larger than 3000 km^2.

3.4 Measurement of snowfall

The reasons that make radar superior to a network of gauges for obtaining areal measurements of rainfall also apply for areal measurements of snowfall. However, the case for using radar to measure snowfall is strengthened by the practical difficulties in obtaining automated measurements of snow depth analogous to those from a network of telemetering raingauges.

The basic principles described in Sec 3.1 whereby measurements of reflectivity may be interpreted in terms of rainfall intensity through an

empirically determined relationship of the form $Z = aR^b$ can be applied to the measurement of snow. One of the limitations in measuring rainfall was the wide range of values for a and b; in the case of snow there is an even larger range of values (Ohtake and Henmi 1970). Gunn and Marshall (1958) give $Z = 2000\ R^{2.0}$. Imai (1960) agree on the exponent but give a range of values for the constant, a, from 540 for dry snow to 2100 for wet snow. Because of this variability, and for the other reasons given in Sec 3.2, it is important that one or more independent "ground truth" estimates of snowfall are used to calibrate the radar.

Only a limited amount of data on the accuracy of radar measurements of snowfall has been obtained. Jatila (1973), using as a calibration the water equivalent of snow collected in a single raingauge, found that 68% of the snowfall amounts derived from radar measurements within a range of 30 km fell in the interval -24% to +32% of the daily amounts of snowfall measured by four check gauges. The most extensive measurements to date have been carried out by Pollock and Wilson (1972). This project used three radars and an extensive gauge network which included 13 weighing recording precipitation gauges (Peck et al, 1973). The accuracy of radar measurements of snowfall was found to be similar to that reported by Jatila within about 30 km of the radar but it rapidly decreased as the height of the radar beam increased with increasing distance from the radar. Both of the above studies were made over flat terrain; however, a recent case study in North Wales by Collier and Larke (1978) showed that comparable accuracy can also be achieved in hilly terrain.

3.5 Measurement of hail size

At the radar wavelengths normally used by meteorologists the power backscattered from rain and snow obeys the Rayleigh backscattering law and the precipitation intensity can be related to the reflectivity factor Z through a simple empirical relationship. When, as in the case of hail, the

particle diameters are larger than one-tenth of the radar wavelength, the back-scattered power is no longer proportional to the sixth power of the particle size. Such particles are in the Mie scattering region where the back-scatter is a complex function of particle size with numerous maxima and minima. In this case, instead of referring to reflectivity factor Z, we use the term equivalent reflectivity factor Z_e, defined as the summation per unit volume of the sixth power of the diameters of spherical water drops in the Rayleigh scattering region that would scatter back the same power as that actually measured. In the presence of a broad spectrum of hail sizes, the maxima and minima in the back-scatter relationship tend to be smoothed out and there is an overall increase in Z_e with hail size especially at 10 cm wavelength. Thus the measurement of $(Z_e)_{max}$ forms the basis of the simplest and most commonly used method of hail detection.

The $(Z_e)_{max}$ approach was pioneered by Donaldson (see his review, 1965); however, he used a wavelength of 3 cm and, probably because of attenuation by liquid water at low levels, he found that it was Z_e measured at high levels in the storm and also the increase of Z_e above the melting level that were the best indicators of hail. More recently, starting with Geotis (1963), measurement of Z_e near the ground at a wavelength of 10 cm has become the more usual hail detection method. Geotis found that 10 cm values of Z_e greater than 3×10^5 mm^6 m^{-3} were almost always an indication of hail. He also found that whenever the maximum hail diameter exceeded 2 cm the maximum Z_e of the storm was above 10^6 mm^6 m^{-3}. Although $(Z_e)_{max}$ is a useful indicator of the probable occurrence of hail somewhere in a storm, it does not give the precise location of the hail within the storm; hail can for example occur in regions of low Z_e within a hailstorm which exhibits a high Z_e in some other part of the storm. Thus there have been a number of investigations into more sophisticated techniques of hail detection. One technique, involving the use of Doppler radars, is described in Sec 6. The

other principle methods are dual wavelength and polarisation techniques.

The value of Z_e for precipitation particles in the Rayleigh region is independent of the wavelength. For particles in the Mie region, however, Z_e shows a strong dependence on wavelength and this was proposed by Atlas and Ludlam (1961) as the basis of an improved method of hail detection. Sulakvelidze et al (1967) claimed success in the detection of hail by comparing values of Z_e measured at approximately 3 and 10 cm, but their approach is suspect since they made no correction for attenuation in deducing Z_e. In an attempt to overcome this difficulty Eccles and Atlas (1973) proposed the use of the range derivative of a quantity y given by the ratio of the Z_e-values measured at 10 and 3 cm. The principle of their method may be understood by reference to Fig 4 which depicts a model storm with a parabolic distribution of rainfall intensity and a hail shaft embedded within it. The parameter y increases monotonically with range in the regions with rain only because of the greater attenuation at a wavelength of 3 cm. However, at the near edge of the hailshaft y increases more rapidly and dy/dr shows a positive spike because the Z_e-value at 10 cm considerably exceeds that at 3 cm. At the far edge of the hailshaft there is a reverse effect. Thus a 'positive hail signal' ($\frac{dy}{dr} > o$) preceding a 'negative hail signal' ($\frac{dy}{dr} < o$) should be characteristic of a hailshaft. Unfortunately, the value of Z_e at different wavelengths is not only a function of the size of the hail; it is also a complex function of the wetness and shape of the hail. In practice, therefore, the situation is not as simple as that shown in Fig 4. Jameson (1975), for example, has shown that inverse hail signals can occur in some circumstances. Some of these problems have been discussed in a review by Srivastava and Jameson (1975). They conclude that a number of problems remain to be resolved before this method can be used with confidence.

Most meteorological radars transmit polarised radiation. The

scattered radiation is depolarised if anisotropic scatterers are involved. The ratio of the orthogonal to the main component of the back-scattered radiation is referred to as the depolarisation ratio. In the case of circular polarisation this ratio is referred to as the CDR, the main component being circularly polarised with the opposite sense of rotation to that transmitted and the orthogonal component being circularly polarised with the same sense of rotation. Calculations of the depolarisation ratio made by Atlas et al (1953) and Barge (1972) using the Rayleigh-Gans theory showed that asphericity may be detected by measurement of the depolarisation. Since hail tends to be aspherical, especially when it is large, this suggested another method for detecting hail. Barge (1972) computed the depoloarisation for observed size distributions and shapes of rain drops and hail. He concluded that most hail should indeed be distinguishable from rain by virtue of greater depolarisation. Results of measurements in several Alberta hailstorms are shown in Fig 5. The full line represents the depolarisation to be expected from rain having a Marshall-Palmer drop size distribution. It is seen that rain often produces greater depolarisation than that predicted theoretically, and therefore depolarisation by itself is evidently not a sufficient criterion for hail detection. One of the problems is that radiation transmitted through an assemblage of anisotropic particles is progressively depolarised so that the radiation incident on particles deep inside a storm may not have the same polarisation as the transmitted radiation (Humphries 1974). Nevertheless, Fig 5 shows that most of the points lying above and to the right of the dotted curve correspond to hail and this supports Barge's (1972) contention that a combination of measurements of CDR and Z_e may be better than Z_e alone as a means of detecting hail.

It has been suggested that it may be possible for damaging hail to be suppressed by cloud seeding methods (eg Sulakvelidze 1967). As a result hail suppression experiments are underway in several parts of the world. The

conduct and evaluation of such experiments depends critically on the ability to monitor the occurrence of hail. Because of the high spatial and temporal variability of hail, it is very difficult to monitor its occurrence by conventional means and so the search for improved methods of radar detection is an important one. Unfortunately, the very variability of hail is itself one of the greatest impediments to acquiring data of sufficient quality to assess the validity of the radar techniques.

4 QUALITATIVE DETERMINATION OF THE DYNAMICAL STRUCTURE OF CLOUD AND PRECIPITATION SYSTEMS

4.1 Measurement of echo shape

In this section we consider what can be learned from the shape of the radar echo from cloud and precipitation systems. The measurement of the shape of such echoes is technically one of the least demanding applications of radar; yet it exploits one of the strongest assets of radar, namely its ability to map effectively instantaneously the 3-dimensional pattern of echo. From the shape of the echo we are able to make deductions about the dynamical mechanisms responsible for the patterns. Although it is usually helpful to be able to distinguish levels of intensity, many of these deductions do not require a high standard of quantitative accuracy in the measurement of the intensity of the radar echo. This is why, even though the deductions may sometimes be subtle in meteorological terms, the necessary radar observations tend to be easier to obtain than are the kinds of measurements discussed in Sec 3.

The three main methods of operating a radar to observe the shape of precipitation systems are:

(a) to scan the beam about a vertical axis to provide plan views at a succession of elevation angles,

(b) to scan the beam in elevation to provide a vertical section at a succession of azimuths, and

(c) to point the beam vertically to obtain a continuous time record of what passes overhead.

Traditionally these data are displayed on a CRT or a facsimile display to give (a) a series of PPI (plan position indicator) displays, (b) RHI (range-height indicator) displays, and (c) a continuous THI (time height indicator) record. Alternatively data from a sequence of PPI-scans can be combined to provide a series of CAPPI (constant altitude PPI) displays at different altitudes (Marshall 1957). In the early years of radar just a single level of intensity was displayed and the receiver gain was adjusted to provide the desired sensitivity; later, with the development of integrating and quantizing devices,(see the review by Atlas 1964), it became usual for several different levels of intensity to be shown together on the CRT or facsimile display as shades of grey. More recently, these kinds of analogue displays have begun to be superceded by digital display techniques. The nature and advantages of these will be discussed later in Sec 5.

We shall draw heavily on pictorial illustration in this section. In fact, we make use of pictures from technically unsophisticated displays, the resulting lack of detail in the pictures being exploited for the sake of clarity of description.

4.2 Patterns of precipitation associated with mid-latitude depressions

Precipitation is generated within moist ascending air and the type of precipitation system depends on the form of dynamical instability responsible for the upward motion. The most basic distinction is between precipitation generated in air that ascends along a gentle 1 in 100 slope over a large area with an upward velocity of the order of 10 cm s^{-1}, and precipitation generated within air that ascends more nearly vertically in localised areas at speeds of several metres per second or more. The first kind of motion is referred to as slantwise ascent and it occurs in frontal, so-called baroclinic, regions where there is a significant horizontal

gradient of temperature. The second kind of motion is simple buoyant vertical convection, hereafter referred to simply as convection. The two kinds of upward motion often coexit, convection occurring when potential instability is released by large scale slantwise ascent. For simplicity, however, Fig 6 shows the appearance of the radar echo in plan view in the extreme cases of (a) uniform precipitation produced by slantwise ascent alone and of (b) showers associated with convection alone.

Precipitation generated by slantwise ascent in the absence of significant convection is characterised by its horizontally stratified appearance when viewed in vertical section. The term stratiform precipitation is sometimes used to describe it. Stratiform precipitation typically gives a well-defined radar 'bright band' associated with the enhanced back-scatter from melting snow (Fig 6 (c)). When pockets of convection occur in regions of large-scale slantwise ascent the vertical radar sections show more irregularity and the bright band becomes less well-defined. Indeed, when the convection is vigorous and extends to high levels, graupel rather than snow becomes the predominant form of frozen precipitation aloft and this does not give rise to any bright band when it melts.

It is common in precipitation systems for the upward motion to become organized into mesoscale bands (eg Nozumi and Arakawa 1967, Browning and Harrold 1969, Browning et al 1973, Houze et al 1976). The resulting precipitation bands tend to be oriented parallel to the baroclinic zones in which they are embedded. They appear to be characterised by transverse circulation patterns which after a while often destabilise the thermal stratification and generate convection within the band. Several different kinds of band can be produced depending on the presence or absence of convection. Fig 7(a), for example, shows parts of two rainbands, each consisting of several mesoscale precipitation areas (MPAs) several tens of kilometres across. Each MPA in this figure consisted of a cluster of

convective cells in which the convective overturning was restricted to a layer about 2 km deep in the middle or upper troposphere (Browning et al 1974). Convection is not always well marked within precipitation bands. In such circumstances the bands tend to be relatively uniform in appearance as in Fig 7(b).

Another, quite different, form of precipitation band is depicted in Fig 7(c). This shows a very narrow band of intense precipitation of the kind often associated with sharp cold fronts (Browning and Pardoe 1973). Vigorous convection occurs in the lowest 3 kilometres in association with such bands and their passage is accompanied by a sharp wind veer. Typically in the British Isles these bands are preceded by a strong low level jet stream, with winds of 25 m s^{-1} or more within a kilometre or so of the surface. Fig 7(c) shows an almost 2-dimensional example of what we refer to as line convection; more often, this kind of convection is broken into line elements (James and Browning 1978).

4.3 Structure of non-precipitating clouds

As discussed in Sec 3.2.5 the optimum wavelength for observing precipitation is 5 cm or longer. Figs 6 and 7, for example, were obtained with 10 cm radars. Except for some ultrasensitive research radars (Sec 7), radars operating at such wavelengths do not detect the small particles within non-precipitating cloud. Because of the inverse-square dependence of the back-scattered radiation on wavelength, however, it is easier to detect such clouds at a wavelength of about 1 cm (referred to as Q-Band in the UK and K-Band in the USA). Ice crystal clouds such as cirrus and altostratus are easiest to detect; clouds composed only of very small water droplets such as fair weather cumulus and altocumulus are detected less often (Harper 1966).

Examples of both water and ice crystal clouds are shown in Fig 8. Fig 8(a) shows a time-height record of altocumulus clouds. Assuming a wind speed of 10 m s^{-1} at cloud level implies that the individual cloud elements

are less than 600 m in horizontal as well as vertical dimensions. The temperature at their altitude, and their blobby as opposed to fibrous appearance, suggests they are water clouds. Clusters of high level precipitation cells are shown in Fig 8(b) with streamers of precipitation falling obliquely beneath them through a region of wind shear. As first demonstrated by Marshall (1953) and his co-workers at McGill University, the nearly vertical echoes in the upper part of the display are ice crystal generating cells; they and their associated streamers travel at the speed of the wind at the level of the generating cells. These generator cells are very weakly convective; vigorous convective cells associated with showers and thunderstorms have an order of magnitude greater horizontal and vertical extent (see Fig 9 later). The flat base of the echo in Fig 8(b) is due to the evaporation of the ice crystals in a dry layer. Occasionally the base of such an evaporating deck of ice crystals has distinct protruberances, sometimes called mammatus, or stalactites (See Fig 8(c)). As proposed by Atlas (1955) and later demonstrated by Harris (1975 a), stalactites are fine-scale convective cells associated with a shallow unstable layer generated by the cooling effect of precipitation evaporating at cloud base. In Sec 6.4 we show that stalactites as pronounced as those in Fig 8(c) can produce intense turbulence.

4.4 Patterns of precipitation associated with severe storms

Rainbands associated with a hurricane were first observed by radar more than three decades ago (Maynard 1945). Thunderstorms were observed intensively using radar as early as 1946 (Byers and Braham 1949) and the first tornado-producing thunderstorm was identified by radar in 1953 (Stout and Huff 1953). A distinctive radar echo pattern was noticed in each case and this was quickly exploited operationally. In countries where damaging storms are common the detection and tracking of such storms remains one of the most important meteorological uses of radar.

Thunderstorms that are intense enough to produce damaging hail and tornadoes are referred to as severe local storms. The most obvious feature of the echo from a severe local storm, apart from high reflectivity due to hail (Sec 3.5), is its great vertical extent. Usually the echo penetrates above the level of the tropopause, as for example in Fig 9. In rough terms, every additional kilometre of penetration indicates an additional 20 m s^{-1} of updraught velocity (eg Vonnegut and Moore 1958). The severity of a thunderstorm is related to the strength of its updraught.

In some areas such as North America severe local storms often occur in lines (squall lines), generally parallel to and ahead of cold fronts. A body of experience has grown up which enables the practiced radar meteorologist to identify the potentially most hazardous portions of these weather systems. One of the most important tasks is to identify which storm cells are likely to be accompanied by tornadoes. A hook echo seen on the PPI display at low elevation angles (Fig 10) is the best-known signature of a tornado. A tornado, if it occurs, will be located neat the apex of the hooked appendage. Unfortunately, the identification of a hook echo is rather subjective. A hook echo is sometimes part of a well-defined and very characteristic three-dimensional echo pattern (Browning 1964) but often it is difficult to identify a hook echo because of limitations of resolution at long range or because of the complexity of the echo patterns produced by interacting cells. Accordingly, although the search for hook echoes is still an important part of operational practice, for the future we look forward to the use of less ambiguous methods of tornado detection using Doppler radar methods (Sec 6.6). We also look forward to the possible use of Doppler radar for measuring wind speeds in Hurricanes or Typhoons (Baynton 1977). But in the meantime the operational use of radar in hurricane situations is limited to the detection of the characteristic spiral rainbands associated with banded regions of updraughts surrounding the hurricane eye (Fig 11).

All the precipitation patterns discussed so far have been interpreted in terms of the nature and distribution of the rising air motion responsible for generating the radar-detected precipitation. Usually the stronger the updraught velocity, the larger are the precipitation particles that are generated and the stronger is the reflectivity of the resulting radar echo. In intense thunderstorms, however, there comes a point when the updraught is so strong that the microphysical factors controlling the conversion of cloud droplets to radar-detectable precipitation particles cannot keep pace with the rate at which the cloud material is swept upwards (see the review by Browning 1978). The result in some severe local storms is that the core of the updraught is characterised by a vault-shaped weak-echo region (Fig 12). In less severe thunderstorms the updraught is still characterised by a weak-echo region (WER) but its extent is limited to the lower parts of the storm. Vaults and WERs in general have taken on increased importance recently as indicators of updraught locations now that research aircraft are beginning to probe the internal structure of intense thunderstorms as part of hail suppression research studies. Moreover, the shape of the WERs and the fine scale features of the surrounding echo are also being exploited to make detailed inferences about the trajectories of precipitation particles that might account for their shape, reflectivity and motion (Browning 1965, Browning and Foote 1976).

The seeding of convective clouds with the aim of either suppressing hail or stimulating rainfall is often conducted nowadays in regions of developing clouds before or during the initiation of precipitation. Often these clouds can be identified visually without difficulty. However, radar can be useful for identifying the time and location of "first echoes" associated with the initiation of the precipitation. The height of the first echoes may also be used to make inferences about the growth mechanism of the particles and about the updraught velocity (see reviews by Battan 1973 and Browning 1977).

5 USE OF RADAR FOR SHORT-PERIOD FORECASTING OF PRECIPITATION

5.1 The philosophy of 'nowcasting'

Most weather forecasts are obtained by first solving the Navier-Stokes equations for the atmosphere by numerical methods (Mason 1973). However, the sporadic nature of the mesoscale instabilities responsible for much of our precipitation limits the capability of numerical methods to predict their onset. Thus there is a lot to be said for the view expressed by Ramage (1976) that the most important step towards achieving detailed forecasts as distinct from present-day forecasts which are couched in rather general terms, would be to use an observing system capable of detecting the mesoscale events at the earliest possible stage. Given such observations, a detailed precipitation forecast for a period up to several hours ahead might then be based on an extrapolation of the observed motion of existing precipitation areas modified by an assessment of the likelihood of intensification or decay arrived at from other meteorological considerations. This approach is sometimes referred to as nowcasting (eg Scofield and Weiss 1976). In this section, we consider how radar can provide the necessary observational data for short-period forecasts of precipitation by simple extrapolation and, then, how radar data together with other numerical or statistical methods might be used to predict changes in the pattern of precipitation.

5.2 Data processing, transmission and display

It has long been known that radar can provide a forecaster with information about the detailed fields of precipitation in a way that no other tool can. In the early 'sixties simple manual extrapolation techniques were already being devised for various kinds of precipitation system (Kessler 1961, Boucher 1963). Operationally, however, radar has tended to be used mainly for the tracking and forecasting of broad features such as squall lines and individual entities such as tornadic storms and hurricane eyes which pose a major hazard. In the case of the detailed pattern of precipitation

the mass of data available was so overwhelming and most of the details of the pattern so perishable, that there was not sufficient time either to analyse or to disseminate more than a crude summary of the major features. Now, with the development of digital techniques and the availability of low-cost mini-computers, this situation is changing. Several programs are underway to develop digital radar processing techniques with a view to the operational measurement and forecasting of precipitation in general. In the USA, for example, there is the D/RADEX program (McGrew 1972). In Britain there is a collaborative project between the Meteorological Office and the Royal Signals and Radar Establishment at Malvern (Taylor and Browning 1974). The essential features of these systems are

(a) A mini-computer at the radar site to take account of the kind of problems described in Sec 3.2 and to convert the radar reflectivity data into quantitative rainfall data in a rectangular Cartesian format.

(b) Transmission of digital rainfall data from the radar site to remote users by low-cost telephone line.

(c) User terminals which enable the quantitative rainfall pattern to be displayed within minutes of real time and at regular intervals either as hard copy print-out as in Fig 13 or, in the case of the Malvern program, on a colour television set.

5.3 Forecasting by simple extrapolation

A feature of the user terminal developed at Malvern is the ability to store and replay speeded-up sequences of precipitation maps on the television set. This 'action replay' facility can be expected to help a forecaster subjectively to extrapolate the motion of the precipitation systems and to identify regions of development and decay. The ideal, however, is to use an objective extrapolation procedure. This can be achieved by applying

computerised pattern metching techniques to the basic digital arrays of data. The use of weather radar data for objective short-period precipitation forecasting was pioneered by Hilst and Russo (1960) even before digital data arrays had become routinely available. They used the displacement of the maximum cross-correlation coefficient between patterns at two times as the extrapolation predictor. They determined the movement of the pattern as a whole and assumed the current pattern would continue to move at this velocity without development. A later refinement of the cross-correlation type of forecast was to identify objectively individual cells and to match the position of each cell with that at previous times (Blackmer, Duda and Reboh, 1973). This is a more complicated procedure because the merging and splitting of cells has to be taken into account. Nevertheless, the added complexity may prove worthwhile because significant variations in velocity do occur between neighbouring precipitation cells especially in the case of severe thunderstorms and orographically enhanced rainfall.

The major drawback of all such techniques is the rapid deterioration in the accuracy of the forecasts as the forecast period is extended. Austin and Bellon (1974), using the simple cross-correlation technique for radar data digitised on a 5 km grid, found that useful predictions of various types of precipitation on this scale could be obtained over periods of only an hour or so. Wilson (1966) found that the time of arrival of individual thunderstorm cells was seldom predictable more than 20 min in advance. Now, a one-hour forecast may be useful for water authorities in some urban areas but, in general, forecasts usually are needed for longer periods than this. One way out of this dilemma is not to attempt to forecast on quite so fine a scale. Although precise forecasts of rainfall over very small areas are thwarted by the rapid development of small-scale features, these developments tend to occur as fluctuations within a more persistent mesoscale area of precipitation (Harrold and Austin 1974). Thus Hill, Whyte and Browning (1977) have suggested that it should be possible to forecast the precipitation over

areas of order 10^3 km^2 for several hours ahead. However, this can be done only if the radar coverage extends sufficiently far upwind of the forecast area. In practice this implies the need for a radar network. A network of radars with partially overlapping coverage has been available in parts of the United States since the 'fifties. Ligda (1957) demonstrated its usefulness for depicting the overall structure of precipitation systems by manually combining the data from different radars in the form of series of montages. For forecasting purposes, however, it is necessary to composite the data automatically and virtually in real time. With the systems described by McGrew (1972) and Taylor and Browning (1974) the compositing can be accomplished fully automatically by computer in the form of a digital map suitable for immediate transmission to users.

5.4 Taking into account development and decay of precipitation systems

To obtain the best possible forecasts we must go beyond the simple linear extrapolation of existing precipitation patterns and attempt to predict their development and decay. There are two kinds of changes to be predicted:

(a) The overall trend as the mesoscale precipitation system goes through its natural life cycle, as influenced for example by large scale forcing, diurnal heating and interaction between mesoscale systems.

(b) Local changes induced by topographical effects, eg orographic enhancement of rainfall over hills and rain shadow effects in the lee of hills.

Consider first the overall trend. Although to a limited extent the trend of intensity can be recognised from the trend in the precipitation patterns observed by radar (Austin and Bellon 1974), to obtain the longer term trends it is necessary to use more traditional meteorological techniques based upon numerical-dynamical models. For forecast periods 12 or

more hours ahead these models are likely to remain the main source of the forecast, with only comparatively small inputs from radar, perhaps to improve the initialisation of the humidity fields or to update the model forecasts in terms of timing and intensity (Moore and Smith 1972). Unfortunately, even the most detailed models now in operational use (eg Bushby and Timpson 1967) have to depend on widely spaced input data and so the intensity, and more importantly the trends in intensity, of mesoscale precipitation events tend to be underestimated (Woodroffe 1976). For forecast periods shorter than 12 hours, precipitation forecasts are likely to depend increasingly on extrapolations from the radar data until, for periods just a few hours ahead, radar becomes the primary source of information in the preparation of the forecast. The exact nature of the mix between numerical-dynamical prediction methods and radar observations, and the extent to which successful mesoscale forecasting procedures can be developed to cope with the difficult 6 to 12 hour period will become clear only after more experience has been acquired with both the radar techniques and with the new breeds of mesoscale numerical models which are now being developed.

We next consider the problem of predicting local topographically induced effects, with particular reference to the problem of forecasting orographic rainfall. Again, one approach is to combine radar data with a numerical-dynamical model, but this time it is necessary for a special fine-scale model to be used which can represent the details of the topography. One such model has been devised by Collier (1975). He used a 1 km grid to represent the topography and attempted to parameterise the physics essential to the production and distribution of precipitation on this scale. His model requires as its input, the temperature, humidity and wind at 10 levels in the atmosphere, together with the surface geostrophic wind and the vertical velocity at 500 mb. These values can be derived from conventional coarse-scale primative-equation models. In its simple form Collier's model tends to overpredict the

rainfall over the hills, essentially because it neglects microphysical and mesoscale factors that prevent the conversion of condensate to rainfall occurring with 100% efficiency. However, by running this model for a hilly area upwind of the area of interest and comparing its predicted rainfall with the actual rainfall measurable by radar, Harrold (1975) was able to derive efficiency factors for different parts of the precipitation system. By assuming that these factors remained constant as the different parts of the systems being tracked by radar approached the forecast area, Harrold was able to obtain a much better forecast of the orographic rainfall when the system finally reached the area of interest.

Another source of information that can be taken into account for predicting topographical effects is the dynamical organisation of a precipitation system as inferred from the shape of the echo pattern (cf Sec 4.2). Much research is needed to classify these effects systematically, but an example of the kind of effect we have in mind is the tendency for sharp surface cold fronts detectable by radar as line convection to demarcate regions experiencing large orographic enhancement of rainfall from regions with small orographic effects (Browning, Pardoe and Hill 1975).

Yet another method of forecasting the modification of precipitation by local topography is to use climatological statistics. Nicholass and Harrold (1975) showed that the amount of rain falling over hilly regions with areas of about 60 km^2 could be predicted with reasonable accuracy from a knowledge of the synoptic weather type and the wind direction at low levels. This result is important because it enables forecasts from coarse-scale numerical models to be used in estimating rainfall over much smaller areas. However, the required statistics can be derived only when rainfall data are available with sufficient resolution. It would be extremely expensive to obtain such data for a large number of regions using autographic raingauges and so the formulation of mesoscale climatological forecasting rules must

in general await the advent of routinely available quantitative radar data.

6 USE OF DOPPLER RADAR FOR THE STUDY OF PRECIPITATION SYSTEMS

6.1 Principles underlying methods of using Doppler radar

Most meteorological radars are noncoherent in the sense that they do not have a very stable transmitter frequency. Such radars are used as described in earlier sections to observe the location and pattern of echoes and to measure the intensity of the backscattered signals. They can also detect the pulse-to-pulse change in signal strength so as to provide estimates of the relative motion of the targets. For many purposes, however, it is useful to measure velocities in absolute terms and for this purpose a coherent radar is required. The name 'Doppler radar' has been given to the class of radar sets which is capable of measuring the shift in microwave frequency caused by moving targets. The first reported meteorological application of Doppler radar (Brantley and Barczys 1957) involved the use of a continuous-wave (CW) radar which was not capable of range discrimination. Recently developments have taken place that enable CW radar to provide both Doppler information and discrimination in range (Strauch et al 1976). However, most of the effort in the past 15 years has been in the development of pulsed Doppler radar systems and of techniques for interpreting the data from them - see, for example, the reviews by Atlas (1964), Lhermitte (1966a, 1969) and Battan (1973).

In this section we shall be concerned only with pulsed Doppler radars. Such radars can measure the spectrum of velocities owing to the populations of precipitation particles within pulse volumes at different ranges. Although the shape of the entire Doppler spectrum is occasionally of interest (see Sec 6.2), for most meteorological applications it is sufficient to determine the first and second moments of the spectrum, ie the mean velocity and the velocity variance. Considerable progress has been made in the development of data processing systems capable of extracting these moments. Although

it is not the purpose of this review to consider the technical details, it is important to realise that the means are now available at reasonably low cost for deriving and displaying them, in real time, simultaneously in a large number of range gates.

There are two important limitations of Doppler radars which influence the manner in which they are used. The first is the problem of range and velocity ambiguities. The product of the maximum unambiguous velocity V_{max} and the maximum unambiguous range r_{max} is equal to $\frac{1}{8}\lambda C$ where λ is the radar wavelength and C is the speed of light. The use of a high pulse repetition frequency (PRF) to enable the unambiguous measurement of high velocities thus restricts the maximum unambiguous operating range. In practice this leads to many Doppler radars being operated at ranges out to only several tens of kilometres. However, a technique using staggered PRF's has been devised to reduce this limitation (Sirmans et al 1976).

The other major limitation of Doppler radars is that they measure only the line-of-sight velocity component of the targets. This has led to the development of a number of distinct ways of using Doppler radar in order to get meteorologically meaningful information. There are 3 main methods. The first and simplest method is to keep the beam fixed and to examine changes in a single velocity component as a function of range and time. This approach is fruitful when the beam is pointed vertically to measure the characteristics of the precipitation targets (Sec 6.2) or at low elevation angles to measure fluctuations in the horizontal wind (Sec 6.4). A second approach, which can be applied when there is a horizontally uniform wind field, is to determine the vector wind velocity by observing precipitation targets at a given altitude with the beam directed along different azimuths (Sec 6.3).

. The data from these two approaches require rather sophisticated meteorological interpretation. Various assumptions have to be made which are valid only in a restricted range of meteorological situations. Accordingly,

these techniques have been confined to rather specialised research studies. The only area in which there is some prospect of an early operational application is in the detection of tornadoes (see Sec 6.6).

A third approach with Doppler radar is to use two or more spaced radars to observe the same precipitation targets from different directions. This can be used to map complex 3-D fields of motion such as those associated with convective storms (Sec 6.5). This method requires fewer meteorological assumptions to be made in the interpretation of the data but is complicated from the point of view of the logistics and the sheer volume of data processing. As a result this method also is limited to special research programs.

6.2 Measurement of the characteristics of precipitation and vertical air motion using a zenith-pointing radar

When the radar beam is pointed vertically the Doppler spectrum within any given pulse volume is the combined result of vertical air motion and the terminal fallspeed spectrum of the precipitation particles (Fig 14). In areas of widespread frontal precipitation the vertical air motion is only of the order of 10 cm s^{-1} and turbulence is often insignificant, in which case the Doppler spectrum can be interpreted straightforwardly in terms of the character of the precipitation. Snow has a narrow terminal fallspeed spectrum, with a mean fallspeed of about 1 m s^{-1}; rain has a broad spectrum with fallspeed varying from 1 to 8 m s^{-1}. Vertical profiles through widespread uniform precipitation thus show a characteristic increase in fallspeed at the melting layer accompanying the reflectivity maximum referred to in Sec. 3.2.3. There is a known relationship between the terminal fallspeed of raindrops and their diameter and so it is possible to infer rain drop size distributions as a function of height (Caton 1966). In the presence of convection, or even without it if there are hills nearby, the vertical air motion often exceeds 1 m s^{-1}. Such updraughts give rise to a displacement of the entire Doppler spectrum. Although, in principle this can be correct for, Rogers (1967)

points out that the interpretation of the Doppler spectrum in terms of drop size distribution is highly sensitive to errors in assumed vertical air motion.

When the beam is in snow, a zenith-pointing radar can be used to provide information on ice particle type (Weiss et al 1976). This method is based on the assumption that very little breakup of precipitation particles occurs within the melting layer. In this case the Doppler spectrum expressed in terms of particle mass should be the same for radar signals returned from just above and just below the melting layer. The power spectrum $P(V_f)$ of particle fallspeed measured with the radar can be converted to the power-weighted mass spectrum $P(M)$ using a relationship between particle mass and terminal fallspeed V_f. A single relationship exists for raindrops but for ice particles V depends on particle type as well as its mass. Thus

$$V_f = aM^b \qquad (3)$$

where a and b take on different values for different ice crystal types (Locatelli and Hobbs, 1974). If the measured power spectrum of velocity above the melting layer is converted to a spectrum of mass $P_A(M)$ using eq (3), the resulting spectrum should match the power spectrum $P_B(M)$ of raindrop mass determined for the region just below the melting layer, provided the proper values of a and b are used. Some indication of the dominant crystal type can thus be inferred indirectly by finding the combination of a and b which gives the closest match between $P_A(M)$ and $P_B(M)$.

We turn now to the determination of vertical air motion using a zenith-pointing Doppler radar. The measurement of vertical air motion is important in meteorology because it determines the rate of condensation within clouds. The displacement of the Doppler spectrum can be assessed in two ways to give a measure of the updraught velocity. The first method, adopted by Probert-Jones and Harper (1961) and Battan (1964), entails the measurement of the minimum fallspeed spectrum bound V_{min} (see Fig 14). Since the smallest

detectable precipitation particles usually have a terminal fallspeed close to 1 m s^{-1}, any departure of V_{min} from this value is taken as a measure of the updraught. The accuracy of the lower-bound method is limited by spectrum broadening produced by turbulence and sometimes also by the inability of the radar and processing equipment to cope with a wide range of intensities. In the presence of rain, a better method of determining the updraught, proposed by Rogers (1964), is to compare the observed mean Doppler velocity ($\overline{V}_r$) with the mean velocity of the terminal fallspeed spectrum ($\overline{V}_f$) calculated from the measured radar reflectivity factor (Z) assuming a Marshall-Palmer dropsize distribution. A further improvement (Joss and Waldvogel 1970) involves the use of an empirical Z-$\overline{V}_f$ relationship instead of assuming a Marshall-Palmer distribution. Rogers (1964) and Joss and Waldvogel (1970) estimate that this technique gives an accuracy of about $\pm$ 1 m s^{-1} in rain; the errors are likely to be rather greater in the presence of hail. Fig 15 shows an example of vertical air velocities derived using both the lower-bound and Rogers' method applied to the same set of data. There is broad agreement in the patterns obtained by the two techniques.

For a more comprehensive review of the use of Doppler radar at vertical incidence the reader is referred to an article by Atlas et al (1973).

6.3 Measurement of airflow at atmospheric fronts

The zenith-pointing mode of operation is capable of giving useful estimates of vertical air velocities of several metres per second in convective clouds but it cannot be used for measuring the widespread slantwise ascending motion associated with fronts, for which the vertical velocities are only of order 10 cm s^{-1}. In this case the vertical velocity is best derived from the divergence of the horizontal wind which can be obtained from a single Doppler radar by means of the conical scanning technique.

Developed successively by Lhermitte and Atlas (1961), Caton (1963) and Browning and Wexler (1968), the conical scanning technique is particularly

valuable where the airflow is horizontally fairly homogeneous over distances of tens of kilometres. In this mode the beam is rotated in azimuth, with the elevation angle (α) kept constant throughout a complete rotation (Fig 16). The line-of-sight velocity of targets (V_r) is measured simultaneously within a number of range positions as they describe circular paths at different altitudes (h). A uniform wind (V_h) would give rise to a maximum component toward the radar when the beam is pointing in the upwind direction, a maximum component away from the radar in the downwind direction, and a zero component in the cross-wind directions; during a complete 360 deg rotation of a single range position a uniform wind would give rise to a sinusoidal velocity-azimuth display (VAD). A more general analysis of the VAD in the case of a non-uniform wind field (Browning and Wexler 1968) shows that:

(i) wind speed (V_h) and direction can be obtained from the amplitude and phase of the first harmonic of the VAD,

(ii) resultant deformation of the horizontal wind field ($def_r V_h$) and the angle of dilatation can be obtained from the amplitude and phase of the second harmonic, and

(iii) divergence of the horizontal wind field (div V_h) can be obtained from the magnitude of the zeroth harmonic after correcting for the effects of precipitation fallspeed (V_f)

All of these kinematic properties are measured as mean values over the area of the scanned circles, which in typical circumstances have diameters of a few tens of kilometres. One parameter that cannot be determined from the VAD is vorticity which would require tangential velocity information around the scanned circles.

The conical scanning technique enables mesoscale horizontal divergence to be measured with an accuracy of typically 5×10^{-5} s^{-1}. By integrating the divergence in the vertical it is possible to determine the vertical air velocity in frontal regions with an accuracy often better than 5 cm s^{-1}.

This kind of accuracy can be achieved only if special precautions are taken to minimise errors, especially those due to variability of precipitation fallspeed. These precautions are discussed by Browning (1971 a) from which it is clear that although this technique can easily be used to measure vertical profiles of the horizontal wind, it must be used with considerable discretion if accurate and representative measurements of vertical air motion are to be obtained.

Many forms of data display are available but, when all that is required is a simple and clear display from which the vertical profile of the horizontal wind can be assessed at a glance, a useful approach is that developed by Sirmans and Doviak (1973) in which shades of grey are used to represent the field of line-of-sight Doppler velocity on a conventional PPI display. An even clearer display is achieved by Baynton et al (1976) using colour television. In both cases pulse pair processing schemes are exploited to derive the mean Doppler velocities in real time. An assessment of the performance of different techniques for deriving the mean Doppler velocity has been given by Sirmans and Bumgarner (1975).

Although the conical scanning technique is the most versatile Doppler technique for studying frontal airflow, it is not suitable for determining the detailed configuration of flow patterns that are highly variable over scales smaller than 10 km. In such cases it is preferable to use a technique in which Doppler velocity is measured simultaneously within a large number of contiguous range positions while the beam is stepped in elevation. This technique was first adopted by Harrold and Browning (1967) who used 80 range positions from 0 to 12 km with 1-deg steps of elevation, from which they were able to construct a detailed field of one component of the velocity within a range-height section (a so-called RHV section). This technique is useful when the principal features of the flow are aligned 2-dimensionally for, by scanning within a vertical section oriented perpendicular to the 2-D system,

it is possible to invoke 2-D continuity to infer the pattern of vertical velocity and the streamlines representing the transverse flow.

An example of the application of both the conical scanning and the RHV techniques is shown in Fig 17, which depicts the pattern of airflow at a cold front. This front has two distinct parts : a region of vigorous line convection at the leading edge of the cold front associated with updraughts of several metres per second (Fig 17 (b)) followed by a region of slantwise ascent with air ascending at a few tens of cm s^{-1} above a gently inclined cold frontal zone (Fig 17 (a)). The pattern of airflow in Fig 17 (a) was derived from a time sequence of conical scans which has been interpreted in terms of a spatial cross section assuming that a steady state circulation was maintained during the passage of the front. The line convection in Fig 17 (b) was measured using RHV scans. The patterns of precipitation associated with the two parts of such a front are quite distinctive, the line convection being revealed by a thin band of intense echo as in Fig 7 (c) and the slantwise ascent by a broad band of less intense echo as in Fig 7 (b).

6.4 Measurement of turbulence

Doppler radar is well suited for measuring turbulence using low inertia particles such as snow to trace the motion (Stackpole 1961). Other precipitation particles can also be used as tracers if only the larger scale wind fluctuations need to be studied. There are two principal ways of using radar for measuring turbulence. One is to measure the mean velocity component in different pulse volumes (typical dimension 100 m) and to investigate changes in that velocity component as a function of distance and/or time. The other, which we consider first, is to measure the variance of the Doppler spectrum σ_v^2 for the return from a single pulse volume. This is given by $\sigma_v^2 = \sigma_1^2 + \sigma_2^2 + \sigma_3^2 + \sigma_4^2$ where the subscripts signify variances due to (1) turbulence, (2) the terminal fallspeed spectrum (3) the wind shear and (4) beam width broadening (as explained by Atlas 1964). σ_4 is generally quite

small and the main problem is to restrict the measurement of turbulence to those meteorological situations where σ_2 and σ_3 can justifiably be neglected. The fallspeed spectrum of snow is quite narrow (Hitschfield and Dennis 1956) and is significantly less than that commonly encountered in turbulence. Thus if a radar is operated in snow with its beam oriented so as to minimize the component of wind shear (either vertically or perpendicular to the wind shear vector), then the spread of the spectrum at any instant can be used as a measure of the intensity of turbulence on scales smaller than the pulse volume (Rogers and Tripp 1964). This technique has been extended to detect regions of severe turbulence within convective storms (eg Frisch and Strauch 1976). Although Frisch and Strauch found from measurements of the gradient of the mean velocity that σ_3 was quite large, they nevertheless found that σ_1 was significantly larger than σ_3 in the regions of severe turbulence that separated the updraughts and downdraughts.

A graphic illustration of the potential of radar for detecting wind fluctuations on scales <u>larger</u> than the pulse length is provided by the photograph of the range-velocity (RV) display shown in Fig 17 (c). This photograph was obtained over a 1-sec period with the radar beam intersecting a sharp cold front at which a 10 m s^{-1} change in the wind component normal to the front occurred within a distance of 1 km. By scanning the beam in elevation to give an RHV section (Sec 6.3) the small-scale structure of velocity pertubations can be resolved in two dimensions. As an example, we show in Fig 18 the results from an RHV scan in a region of intense turbulence which accompanied a stalactite formation similar to that shown in Fig 8(c) (cf Sec 4.3).

Doppler radar techniques have been employed extensively by Gorelik and his colleagues at the Central Aerological Observatory in Moscow to measure the spectral characteristics of turbulence in both precipitation and clear air. Fixed-beam techniques were used to derive structure functions from the time changes of the mean velocity within individual pulse volumes and from

the differences in velocity between different ranges (eg Mel'nichuk 1971). They also derived quantities such as rms velocity fluctuation, and eddy dissipation rate. Lhermitte (1968 a), D A Wilson (1970) and Bryant and Browning (1975) have made use of the turbulent fluctuations observed during conical scans. They were able to evaluate turbulence spectra as a function of height for both horizontal wind components and the covariances $\overline{u'w'}$ and $\overline{v'w'}$. The effect of the covariance terms, which express the vertical flux of momentum, can be distinguished in the conical scans from that due to the terms $\overline{u'}^2$ and $\overline{v'}^2$ because, in the presence of a homogeneous field of motion, they contribute to the measured velocity fluctuations in opposite senses on opposite sides of the scanned circle. This technique must, however, be used with caution since spurious results are likely to be produced if either the distribution of target fallspeeds or the turbulence field itself is not horizontally homogeneous (Harris 1975 b).

6.5 Use of multiple Doppler techniques to measure the 3-D structure of convective storms

The limitation of a single Doppler radar to the measurement of only a single component of motion at any given point is most restrictive in the case of the complex fields of motion within convective storms. If we are content with simple measurements of updraught velocities in a small portion of a storm then a single zenith pointing radar may suffice (Sec 6.2), but for many research purposes it is necessary to derive the full 3-D pattern of air motion. There have been some attempts to make sensible interpretations of the data from one Doppler radar in terms of the overall airflow pattern, but these tend to invoke numbers of unsupportable meteorological assumptions. In these cases there can be no escaping the need to deploy more than one Doppler radar. One technique which has been used quite extensively involves the simultaneous deployment of two Doppler radars. Another, of which there has been less experience, involves using three

Doppler radars. We consider first the dual-Doppler method, using the so-called coplane method of scanning and data reduction.

The coplane method was proposed by Lhermitte and Miller (1970) and has been described thoroughly with error analysis by Miller and Strauch (1974). The two radars are separated by a distance of typically 40 km and made to scan a common volume in such a way as to minimise everywhere the interval between each volume being scanned by the two radars. This is achieved by scanning the two radars simultaneously in a common plane (the coplane) which is inclined above the local horizontal but passes through the positions of the two radars. By scanning coplanes sequentially at a series of elevation angles a 3-D scan of the entire storm is obtained over a period of 2 to 5 min depending on the range of the storm. According to Miller (1972), the data should be analysed in a cylindrical co-ordinate system. Radial velocity estimates from the two radars are combined, after correcting for the component due to the terminal fallspeed of the precipitation targets using Rogers' (1964) method, to give the 2-D field of motion in each coplane. Airflow normal to the coplane is then obtained from 3-D continuity considerations. The 3 coplane components can then be transformed to the required horizontal and vertical wind components at Cartesian grid locations. A limitation of this technique is that it is necessary to integrate up from ground level to derive the wind field aloft. This prevents measurements from being made above weak echo regions (cf Sec 4.4) unless independent measurements of vertical velocity are available.

The coplane method is particularly well suited to studying the dynamics of convective storms (see for example the results published by Miller 1975, Ray et al 1975, Kropfli and Miller 1976) but it can also be applied to derive 3-D fields of motion in other kinds of situation (see eg Frisch et al 1974). Portrayal and interpretation of the resulting 3-D fields of air motion is an art in itself; however, the vertical section in Fig 19, which is one of a

number of sections derived by Kropfli and Miller (1976) through a Colorado hailstorm, serves to illustrate the potential of this technique.

Lhermitte (1968 b) has carried the multiple-Doppler concept to its logical conclusion by proposing the simultaneous use of 3 radars to scan the same storm. In this way three simultaneous equations can be solved for the radial velocities from three different directions at each x, y, z position within the storm. This permits the calculation at each point of the horizontal wind components u and v and also a quantity which is equal to the sum of the vertical air motion w and the mean reflectivity-weighted terminal fallspeed of the precipitation particles. The value of w can be derived from the 3-D continuity equation knowing the 3-D distribution of u and v and this enables the 3-D distribution of the mean terminal fallspeed of the particles to be derived in addition to the field of air motion. Although the inferred particle fallspeeds are subject to large errors at low altitudes, Bohne and Srivastava (1976) estimate that this technique can provide a useful indication of the size and distribution of hailstones within the upper parts of a storm. Browning and Atlas (1977) stress the value of such measurements for deducing the trajectories of growing hailstones in storms: this sort of information is important for understanding hailgrowth mechanisms and for the evaluation of hail suppression experiments.

6.6 Detection of tornadoes

A tornado circulation was first detected by Doppler radar in 1958 (Smith and Holmes 1961). This early observation was made with a continuous wave radar and there was no way of distinguishing the distance of the tornado from the radar. The great potential of pulsed Doppler radar for locating tornadoes was recognised, however, and its use as a tornado warning tool was advocated by Lhermitte (1964) and by Atlas (1963) who pointed out that Doppler measurements could be expected to provide a much less ambiguous tornado signature than the hook echoes discussed in Sec 4.3.

There are two ways in which one might use a Doppler radar to detect a tornado. Both assume the presence of targets such as precipitation particles to trace the motion, an assumption which sometimes breaks down at low levels but is likely to be valid usually at higher levels. The first method involves the identification of changes in the mean Doppler velocity (ie the first moment of the Doppler spectrum) from one pulse volume to the next as the radar beam is scanned in azimuth. Any significant localized azimuthal shear revealed in this way can be taken as indicative of a vortex large compared with the radar pulse volume. Such a vortex would correspond to the parent circulation, or mesocyclone, from which the tornado itself is spawned. The other method entails the identification of an abnormally broad Doppler spectrum (the second moment of the Doppler spectrum) indicative of strong shear associated with that part of the tornado circulation occurring within the pulse volume itself. The majority of studies have concentrated on the first of these techniques. To some extent this is because the maximum unambiguous range of velocity that can be distinguished by most Doppler radars is small compared with the spread of velocities encountered in and near tornadoes. One of the few studies concerned primarily with the measurement of the second moment (Zrnic and Doviak 1975) demonstrated that large spectrum widths did indeed occur in the vicinity of a tornado but the precise location of the tornado could not be pin-pointed.

The development of methods of using Doppler radar for tornado detection has had to await the development of methods for deriving and displaying the moments of the Doppler spectrum in real time. One of the earliest methods was based on the Coherent Memory Filter (Chimera 1960; Groginsky 1965). This provided a real-time estimate of the first and second moments simultaneously over a large number of range elements. The output of this device was used by Armstrong and Donaldson (1969) who displayed it on an ordinary PPI scope

which they then referred to as a Plan Shear Indicator (PSI). The resulting pattern on the PSI display is a series of concentric arcs, each one being located on the display at its appropriate range plus an incremental displacement which depends on the radial component of velocity at that range. Tangential shear associated with a vortex is revealed by wrinkles in these arcs.

Further advances in real-time processing techniques have been made by Rummler (1968) and Sirmans and Doviak (1973). These new methods have the advantage of high accuracy, small memory requirements, and computational efficiency and therefore relatively low cost. Along with these techniques, improved methods of displaying the first moment have been developed by Sirmans and Doviak (1973) and Gray et al (1975) in which velocities are represented by shades of grey and colours, respectively. A way has also been found of simultaneously displaying 2-dimensional fields of both the first and second moments as well as of the reflectivity (Burgess et al 1976).

In parallel with these technological advances, experience has been accumulating in the application of Doppler radar to the detection of tornado vortices. As noted above, most of the studies have been concerned with the detection of circulations on scales large compared with the radar pulse volume. Donaldson (1970) confirmed that a tornado vortex may be identified from the large values of tangential shear, defined as the gradient of Doppler velocity normal to the radar beam. A recent example of such a tornado vortex signature (TVS) is shown in Fig 20. Donaldson found that the shear pattern associated with a tornado vortex extends vertically to a height greater than its diameter and that the shear pattern remains localized and well-defined when viewed from different azimuths. He found (1971) that a change in the Doppler velocity of 20 m s^{-1} along a distance of 1 km normal to the radar beam was a threshold for identifying storms severe enough to produce damaging

winds and/or large hail. In a one-year period of observations, Sirmans et al (1974) observed several tens of storms with Doppler radar for evidence of a TVS. Only 9 storms revealed evidence of a resolvable TVS; tornadoes were reported in 7 of these. Storms that did not show any evidence of a TVS did not produce any confirmed tornadoes.

One of the most attractive possibilities offered by Doppler radar is of a substantial warning of severe events on the ground through earlier detection of a vortex aloft. Donaldson (1975) reported an example of a TVS which was first noted aloft between 5 and 8 km as much as 40 mins before the tornado touched down. Similar reports of the detection of vortices aloft 40 to 60 mins before the occurrence of funnel clouds, tornadoes and surface wind damage have also been reported by Brown et al (1971), Brown et al (1975) and Donaldson et al (1975).

7 USE OF RADAR TO PROBE THE STRUCTURE OF THE OPTICALLY CLEAR ATMOSPHERE

7.1 Nature of clear air echoes

Reports of radar echoes from the optically clear atmosphere in the absence of both cloud and precipitation date back almost to the time when radar was first used. Since then radars of greater power and sensitivity have detected clear air echoes with increasing frequency. Because of the absence of targets readily detectable by visual means, these echoes came to be known as angel echoes. For many years a lively controversy existed between one school of thought (eg Atlas 1960; Lane and Meadows 1963) which contended that angel echoes were due to inhomogeneities of refractive index associated with sharp gradients of temperature and humidity, and another school of thought (eg Crawford 1949; Harper 1960) which contended that they were due to birds or insects. We now know that both interpretations can be correct. In a review article by Hardy and Katz (1969), angel echoes are

classified into two broad categories : (1) dot angels and (2) angels having substantial lateral or vertical extent. The first category can be ascribed almost entirely to the backscattering by discrete, single targets such as birds or insects. The second category can usually be attributed to inhomogeneities of refractive index but may occasionally be produced by large concentrations of birds or insects dispersed in such a way that their spacings are less than the radar resolution.

There is considerable circumstantial evidence to support this classification, but the most decisive evidence was obtained in a series of experiments at Wallops Island, Virginia, in which the optically clear atmosphere was observed simultaneously with ultrasensitive radars at wavelengths of approximately 3, 10 and 70 cm. Hardy, Atlas and Glover (1966) found that, at ranges close enough to resolve individual targets, the wavelength dependence of the cross-section of dot angles between 10 and 70 cm was close to the λ^{-4} law for Rayleigh scattering from point targets. In the case of the extended targets, however, the wavelength dependence was almost negligible, in keeping with the $\lambda^{-1/3}$ relationship derived by Tatarski (1961), Smith and Rogers (1963) and Atlas et al (1966). All of these workers assumed that the backscattered energy is from refractive index inhomogeneities generated by isotropic homogeneous turbulence in the inertial subrange for which the one-dimensional fluctuation spectrum is proportional to $K^{-5/3}$ where K is the wavenumber.

The theory which accounts for the backscattering from turbulence in the inertial subrange has been reviewed by Watkins & Browning (1973). Although it seems to account well for the observed results, there are still some unresolved problems. For example, it is generally accepted that clear air echoes come from layers of high static stability for which the concept of an inertial subrange is of questionable validity. Indeed, high-resolution refractometer measurements (Lane 1969) indicate that the slope of the

refractivity spectra in such layers is often substantially steeper than $K^{-5/3}$ at the small scales (half the radar wavelength) which give rise to the radar echo.

Even if the detailed physics of the backscatter from refractively turbulent regions of the atmosphere is open to doubt, the meteorologist can still gain much valuable information by adopting a pragmatic approach. Whatever the detailed mechanism of generation of the clear air echoes the fact remains that they serve as tracers of a large number of important atmospheric phenomena that are otherwise difficult to observe. The techniques used resemble those described in earlier sections, namely the interpretation of the intensity, shape, and Doppler shift of the returned echoes. The chief difference is the requirement for radars of high sensitivity. This can be achieved either by using ordinary pulsed radars with powerful transmitters, low-noise receivers, and large high-gain aerials (eg the Wallops Island radars described by Hardy et al 1966 or the Defford radar described by Watkins 1971) or by using frequency modulated continuous wave (FMCW) radars (eg the radars at the Navel Electronics Laboratory Center described by Richter 1969 or at the Wave Propagation Laboratory described by Bean et al 1971). The FMCW radars have a modest transmitted power but high range resolution and the effective sensitivity is achieved by being able to fill the beam with regions of high reflectivity which according to Atlas et al (1970) are often only a few metres deep in the case of clear air echoes. In the remainder of this section we outline some of the principal applications of these radars. Only a few radars exist which are suitable for clear air measurements and their use has so far been limited to specialized research studies.

7.2 Detection of atmospheric stratification

One of the earliest observations of clear air layer echoes was made by Lane and Meadows (1963). They showed that the layer echo was associated

with a sharp vertical gradient of refractive index associated with a stably stratified layer. Not long afterwards the tropopause layer was detected by Atlas et al (1966). In fact ultrasensitive radars operating at wavelengths of order 10 cm often detect stable layers simultaneously at many heights (Fig 21) for it seems that, just as is the case in the ocean thermocline (Woods 1968), the atmosphere consists of large numbers of stably stratified thin sheets separating somewhat thicker layers of lower stability. The statically stable sheets tend to be regions of strong shear and this leads to local dynamic instabilities which create microscale turbulence within the sheets. It is the action of the microscale turbulence in stirring up the mean local gradient of refractive index that is responsible for the backscattered radar signal.

The existence of stable atmospheric stratification as revealed in pictures such as Fig 21 is of interest to communications engineers because of its effect on EM propagation. The layered structure detected by radar is also of interest to the meteorologist because the purturbations in the layers reveal significant features of the dynamics of the atmosphere. One example, illustrated by Fig 22, is the distortion of the flow by lee waves. The clear air echo layers centred at 2 and 3 km altitude can be seen to have a crest-to-trough amplitude of 600 m and a wavelength of 20 km at ranges between 50 and 70 km from the radar. These waves were produced where a strong westerly flow was crossing the Welsh hills west of the radar. Using data of this kind, Starr and Browning (1972) found that the radar was able to reveal substantial variations in wave amplitude sometimes over quite small time scales which would have been impossible to predict in the traditional way on the basis of radiosonde data.

Echo layers are also sometimes perturbed by shearing instabilities leading to breaking-wave patterns. These are responsible for the phenomenon of clear air turbulence and will be discussed in Sec 7.6.

7.3 Detection of air-mass boundaries

Some of the earliest detections of air-mass boundaries were by Newell (1958) and Atlas (1960). They observed lines of clear air echoes associated with sea breeze fronts. Atlas reported that the refractive index dropped by 30 N units as the front passed by, suggesting that refractive index inhomogeneities were responsible for the echo. In later studies of echoes from sea breeze fronts (Geotis 1964), it was considered that birds and insects were the more likely source of the echoes. Simpson, Mansfield and Milford (1977) suggest that both sources of echo can coexist.

Similar lines of echoes have been detected at the leading edge of the cold outflows associated with thunderstorms and cold fronts (eg Fig 23). Again there were some observers who attributed the echoes to refractive index inhomogeneities (eg Leach 1957, Luckenback 1958; Brown 1960) and others to birds congregating in regions of convergence where rising air was carrying insects aloft (eg Harper 1958, 1960). All agree that the echo is associated with the air mass boundary, however, and so to the meteorologist these are useful observations regardless of the nature of the scatterers.

7.4 Measurement of the structure of convection in the boundary layer

Some of the earliest radar observations of convection in the boundary layer were made by Harper, Ludlam and Saunders (1957) and Atlas (1959) who in scanning the radar in the vertical observed inverted U-shaped echoes corresponding to the tops and edges of cumulus clouds. Since the ultra-sensitive radars at Wallops Island and Defford have become available these kinds of echoes have been detected frequently both in the presence of cumulus clouds and in cloudless conditions. An example is shown in Fig 24. When the radar is scanned about a vertical axis with the elevation angle adjusted such that the beam intersects the edges of the convective elements, characteristic ring or doughnut-shaped echoes are observed. Some of the clearest ring echoes have been observed with the Wallops Island radars during outbreaks of

cold air over the warm sea. An example is shown in Fig 25. The ring echoes are best observed when the radar scans close to the top of the convective elements where ascending air overshoots its equilibrium level to become colder than the surrounding air at its level. The combination of relatively high humidity and low temperature within the tops of these elements where they penetrate into dry warm air above the boundary layer gives rise to large refractive index gradients and hence strong clear air echoes at their upper boundaries. When the wind is not too light the convective cells may become organized into rows oriented almost parallel to the wind (Hardy and Ottersten 1969, Konrad 1970). The spacing of these rows is similar to that predicted by Faller (1965).

7.5 Measurement of variations in the depth of the boundary layer

Observations with the ultrasensitive Defford radar have shown that on some days the echoes from the top of the convective boundary layer can be detected almost continuously out to ranges as large as 100 km (Harrold and Browning 1971). By scanning the radar beam in elevation at a succession of azimuths it is thus possible to map the depth of the boundary layer over quite a large area. Harrold and Browning observed that there were mesoscale areas of deeper convection (ADCs) some tens of kilometres across which sometimes could be tracked over periods of several hours. On days of weak winds these ADCs were clearly related to the topography. For example, Fig 26 shows that just after noon on one summer day the boundary layer was three times deeper over an area of land 200 m or more above sea level (the Cotswolds) than it was in a neighbouring valley (the Severn Estuary). The ADC over the Cotswolds on this occasion continued to deepen until four hours later the convection was able to penetrate the capping stable layer and generate thunderstorms. Observations such as this might be particularly useful for identifying the regions of low-level convergence that precede the outbreak of severe thunderstorms in areas like the United States mid-west where the storms represent a considerable threat to life and property.

Harrold and Browning (1971) concentrated on mapping the broad spatial distribution of the depth of the evolving boundary layer. Other studies have exploited radar techniques to observe the evolution of the boundary layer locally and in more detail. Browning, Starr and Whyman (1972a) and Readings, Golton and Browning (1972) have combined observations from the Defford radar with fast-response turbulence probes suspended from a tethered balloon with the purpose of investigating the dynamical mechanisms at the top of the boundary layer that account for the transfer of heat and mass across it. They identified shearing instabilities at the crests of convective circulations as one important transfer mechanism .

In order to study the mixing mechanisms in the boundary layer it is desirable to be able to observe the pattern of echo down to very small scales. However, the resolution obtainable with ultrasensitive pulsed radars has until recently been limited to about 150 m in range. Accordingly much of the fine detail of the convective structures has gone undetected. Improved resolution can be achieved using pulse compression techniques (eg Fetter 1970) but in practice the resolution can be improved by only an order of magnitude. Substantially better resolution, about 1 m in range, has been achieved by Richter (1969) using FMCW radar. An example of the finescale structure observable with fixed zenith-pointing FMCW radars is shown in Fig 27. Two records are shown. One shows a shallow 200 m deep layer of cold moist air as it came ashore after crossing the cold sea surface off southern California. The other shows the deeper layer with well-developed convection after the same airstream had penetrated 5 km inland. The erosion of the initially rather uniform capping inversion as the cold air travelled over warm land is very evident in Fig 27.

7.6 Detection of clear air turbulence

Clear air turbulence (CAT) in the free atmosphere is chiefly a manifestation of Kelvin-Helmholtz (KH) instability (Roach 1972). This is a

form of dynamic instability produced within a hydrostatically stable flow in the presence of sufficiently strong vertical shear. It appears as amplifying waves ("billows") oriented perpendicular to the shear vector, into which the vorticity is concentrated, and which eventually "break" into turbulent flow on a range of smaller scales. The KH billows are detectable by radar from the way in which they distort and intensify thin layers of echo. The amplitude of the billows varies from metres to hundreds of metres. In the case of the commonly occurring small-amplitude billows, the distortion of the layer may not be resolvable by radar; however, the mere presence of the echo is suspected as being due to the effect of the billows (Ottersten 1970). Occasionally, though, especially in the vicinity of upper tropospheric jet streams where the shear is strong over a deep layer, large-amplitude billows develop which are easily resolvable by radar, as shown in Fig 28.

The appearance of the echo pattern in Fig 28 has been likened to that of a braided rope (Hicks and Angell 1968). Such a pattern represents one stage in the evolution of the instability. Observations of the entire life cycle are unfortunately difficult to obtain. In one case, reported by Browning and Watkins (1970), a train of large-amplitude billows was observed by radar to develop to maturity in a period of about 10 min. Rawinsonde measurements in the vicinity of large-amplitude billows (Browning 1971b) indicate that the Richardson number over the layer occupied by the billows tends to be close to $\frac{1}{4}$ which, according to Miles and Howard (1964), is the critical value for the onset of KH instability. Convincing evidence that such billows are indeed associated with CAT has been obtained by flying meteorologically instrumented aircraft through regions simultaneously being probed by ground-based radar (Browning et al 1970; Hardy, Reed and Mather 1973).

Only the more intense CAT tends to be associated with large-amplitude billows of the kind portrayed in Fig 28. Thus there has been considerable effort to devise more widely applicable methods of CAT detection. Atlas, Hardy and Naito (1966) and Hardy, Atlas and Glover (1966) have shown that the intensity of the turbulence can be expressed by a parameter C_n^2 which should be directly proportional to the reflectivity of the clear air echoes. Measurements of radar reflectivity made in conjunction with a large number of aircraft measurements support the validity of this approach by demonstrating that CAT always existed in the vicinity of clear air echoes and that, although not all CAT gave a detectible echo, intense CAT was consistently more likely to be detected than weak CAT (Glover et al 1969; Glover and Duquette 1970). One of the problems of using radar reflectivity as a measure of CAT intensity, however, is the difficulty in objectively distinguishing clear air echoes from precipitation echoes without resorting to multi-wavelength measurements. Accordingly, a better approach is to measure fluctuations in wind velocity directly from the Doppler characteristics of the radar echo as described in Sec 7.7.

It would be wrong to suppose that high-power radar is likely to play a major role as an operational CAT detector. A single radar of the kind used at Wallops Island or Defford can detect significant CAT throughout the troposphere to ranges of only about 30 km and so a network of radars giving coverage over a large area would be prohibitively expensive. In any case, the primary operational requirement is for a CAT detector small enough to be carried on board an aircraft and, as pointed out by Watkins and Browning (1973), this is beyond the state of the art. The great value of high-power radar is, rather, as a research tool for investigating the physics of atmospheric instabilities

7.7 Quantitative determination of winds and wind shear in the clear air

Early studies in this area concentrated on the application of pulsed Doppler techniques using clear air returns in the atmospheric boundary layer.

Browning and Atlas (1966) and Lhermitte (1966b) used the conical scanning technique (Sec 6.3) to obtain vertical profiles of the wind in the clear air up to almost 1½ km. However, they used insects as tracers and, although Lhermitte found that such tracers were often abundant in Oklahoma, insects in general cannot be considered a reliable source of echo. Recently frequency-modulated continuous-wave (FMCW) radar techniques have been developed to measure Doppler velocities (Strauch et al 1976). Chadwick et al (1976) demonstrated that this approach provides a reliable means of measuring winds up to a height of 1 or 2 km using echoes from refractive index inhomogeneities. Since this technique can also provide measurements at ranges as close as 30 m, at low cost, and in precipitation as well as in clear air, FMCW radar has the potential to become a valuable tool for measuring low-level wind shear operationally at airfields.

The development of Doppler facilities on high-power radars has enabled clear air velocity measurements to be extended to much higher altitudes (Browning et al 1972b). However, these measurements can be made only within discrete echo layers (such as those shown in Fig 28) and not at all heights simultaneously. The main application of these measurements is for research investigations of the detailed pattern of velocity within individual echoes. For example, in a study of large-amplitude KH billows, Browning et al (1973) were able to identify a train of vortices in which each vortex was characterised by a vertical shear of 6 m s^{-1} (100 m)$^{-1}$ corresponding to twice the magnitude of the shear between the vortices. This provided a valuable frame of reference for the interpretation of simultaneous measurements from an aircraft flying through the billows.

8 CLOSING REMARKS

One has only to glance at the Table of Contents to appreciate the broad range of applications of radar in meteorology. Progress in the development of new techniques has, as described above, been rapid in many of these areas over the last 15 years. However, the versatility of radar and the very

abundance of data it provides, may in one sense have impeded its operational application, for there is still (as Kessler put it in 1961) 'an undesirable tendency on the part of many radar-weather specialists to think in terms of what the radar alone can do'. Continued rapid progress depends as much on improved integration of radar with other meteorological techniques as it does on the further development and refinement of the radar techniques themselves. To quote Johnson (1973), we particularly need to exploit new technology 'for processing, interpreting, disseminating and displaying meteorological data as a merged whole.' In this way we can expect that the present gap between research and operational application will be narrowed.

REFERENCES

Abshaev M T, 1971 Radar Meteorology : Proc.3rd All-Union Conf Radar Meteor Translated from Russian, Israel Program for Sci Translations, (Jerusalem Keter Press) pp 80-96.

Armstrong G M and Donaldson R J Jr, 1969 J Appl Meteor 8 376-383.

Atlas D, 1955 Proc 5th Weather Radar Conf. Am. Meteor Soc. Boston 321-328.

Atlas D, 1959 J Meteor, 16 6-11

Atlas D, 1960 J Meteor, 17 244-258.

Atlas D, 1963 Bull Am Meteor Soc, 44 772-777.

Atlas D, 1964 Advances in Radar Meteorology, In Advances in Geophys, 10 (New York Academic Press) pp 318-478.

Atlas D, Hardy K R, Glover K M, Katz I and Konrad T G, 1966 Science, 153 1110-1112.

Atlas D, Hardy K R and Naito K, 1966 J Appl Meteor, 5 450-460.

Atlas D, Kerker M and Hitschfeld W, 1953 J Atmos Terrest Phys, 3 108-119.

Atlas D and Ludlam F H, 1961 QJR Meteor Soc, 87 523-534.

Atlas D, Metcalf J I, Richter J H and Gossard E E, 1970 J Atmos Sci, 903-913.

Atlas D, Scivastava R C and Sekhon R S, 1973 Rev of Geophys and Space Phys, 11 1-35.

Atlas D and Ulbrich C W, 1974 J Rech Atmos, 8 275-298.

Atlas D and Ulbrich C W, 1976 Preprints 17th Radar Meteor Conf, Am Meteor Soc, Boston 406-413.

Austin G L and Bellon A, 1974 QJR Meteor Soc, 100 658-664.

Austin P M, 1964 Proc 11th Weather Radar Conf, Am Meteor Soc Boston 166-171.

Bader M J and Roach W T, 1977 QJR Meteor Soc, 103 269-280.

Barge B L, 1972 Scientific Report MW-71 Stormy Weather Group, McGill Univ Montreal 80 pp.

Battan L J, 1964 J Appl Meteor, 3 415-420.

Battan L J, 1973 Radar Observation of the Atmosphere (University of Chicago Press).

Battan L J and Theiss J B, 1970 J Atmos Sci, 27 293-298.

Baynton H W, 1977 Report prepared for Monitoring and Assessment Research Centre, University of London.

Baynton H W, Frush C L, Serafin R J, Hobbs P V, Houze R A Jr and Locatelli J D, 1976 Preprints 17th Radar Meteor Conf Am Meteor Soc Boston 232-238.

Bean B R and Dutton E J, 1968 Radio Meteorology (New York: Dover)

Bean B R, McGavin R E, Chadwick R B and Warner B D, 1971 Boundary-Layer Meteor, 1 466-473.

Blackmer R H Jr, Duda R O and Reboh R, 1973 Final Report, Contract 1-36072 Stanford Res Inst, Menlo Park, California.

Bohne A R and Srwastava R C 1976 Preprints 17th Radar Meteor Conf Am Meteor Soc Boston 7-14.

Boucher R J, 1963 Proc 10th Weather Radar Conf Am Meteor Soc Boston 1-7.

Brantley J Q and Barczys D A, 1957 Proc 6th Weather Radar Conf Am Meteor Soc Boston 297-306.

Brown H A, 1960 Proc 8th Weather Radar Conf Am Meteor Soc Boston 65-72.

Brown R A, Bumgarner W C, Crawford K C and Sirmans D, 1971 Bull Am Meteor Soc, 52 1186-1188.

Brown R A, Burgess D W, Carter J K, Lemon L R and Sirmans D, 1975 Bull Am Meteor Soc, 56 524-526.

Browning K A, 1964 J Atmos Sci, 21 634-639.

Browning K A, 1965 J Atmos Sci, 22 669-677.

Browning K A, 1971 a Weather, 26 293-304 and 320-340.

Browning K A, 1971 b QJR Meteor Soc, 97 283-299.

Browning K A, 1972 Weather, 27 2-13.

Browning K A, 1977 The Structure and Mechanisms of Hailstorms. In Meteor Monograph Am Meteor Soc Boston To be published.

Browning K A, 1978 The General circulation of thunderstorms Part II, Chapter 5, In Thunderstorms - A Social, Scientific and Technological Documentary Ed E Kessler (University of Oklahoma Press) To be published.

Browning K A and Atlas D 1966 J Atmos Sci, 23 592-604.

Browning K A and Atlas D, 1977 J Appl Meteor, 16 327-332.

Browning K A, Bryant G W, Starr J R and Axford D N, 1973 QJR Meteor Soc, 99 608-618.

Browning K A and Foote G B, 1976 QJR Meteor Soc, 102 499-533.

Browning K A, Hardman M E, Harrold T W and Pardoe C W, 1973 QJR Meteor Soc, 99 215-231.

Browning K A and Harrold T W, 1969 QJR Meteor Soc, 95 288-309.

Browning K A and Harrold T W, 1970 QJR Meteor Soc, 96 369-389.

Browning K A, Hill F F and Pardoe C W, 1974 QJR Meteor Soc, 100 309-330.

Browning K A and Pardoe C W, 1973 QJR Meteor Soc, 99 619-638.

Browning K A, Pardoe C W and Hill F F, 1975 QJR Meteor Soc, 101 333-352.

Browning K A, Starr J R and Whyman A J, 1972 a Boundary-Layer Meteor, 4 91-111.

Browning K A, Starr J R and Whyman A J, 1972 b Nature, 239 267-269.

Browning K A and Watkins C D, 1970 Nature, 227 260-263.

Browning K A, Watkins C D, Starr J R and McPherson A, 1970 Nature, 228 1065-1067.

Browning K A and Wexler R, 1968 J Appl Meteor, 7 105-113.

Bryant G W and Browning K A, 1975 QJR Meteor Soc, 101 35-54.

Burgess D W, Hennington L D, Doviak R J and Ray P S, 1976 J Appl Meteor, 15 1302-1306.

Burgess D W, Lemon L R, and Brown R A, 1975 Preprints 16th Radar Meteor Conf Am Meteor Soc Boston 99-106.

Busby F H and Timpson M S, 1967 QJR Meteor Soc, 93 1-17.

Byers H R and Braham R R Jr. 1949 The Thunderstorm (Washington DC: Government Printing Office).

Carbone R E, Atlas D, Eccles P J, Fetter R and Mueller E, 1973 Bull Am Meteor Soc, 54 921-924.

Caton P G F, 1963 Proc 10th Weather Radar Conf Am Meteor Soc Boston 290-296.

Caton P G F, 1966 QJR Meteor Soc, 92 15-30.

Chadwick R B, Campbell W C, Moran K P and Strauch R G 1976 Preprints 17th Radar Meteor Conf Am Meteor Soc Boston 326-329.

Chimera A J, 1960 Final Report (Appendix C) Contract No. AF 33(616)-6352 Buffalo N Y : Cornell Aero Labs.

Collier C G, 1975 QJR Meteor Soc, 101 407-422.

Collier C G, 1976 Meteor Mag, 105 381-392.

Collier C G, 1977 Proc World Meteor Org. Tech Conf on Instruments & Methods of Observation, Hamburg.

Collier C G and Larke P R, 1978 Meteor Mag, 107 To be published.

Collis R T H and Ligda, 1961 Proc 9th Weather Radar Conf, Am Meteor Soc, Boston 391-395.

Crawford A B, 1949 Proc Inst Radio Eng, 37 404-405.

Donaldson R J Jr, 1965 Bull Am Meteor Soc, 46 174-193.

Donaldson R J Jr, 1970 J Appl Meteor, 9 661-670.

Donaldson R J Jr, 1971 Preprints 7th Conf on Severe Local Storms, AM Meteor Soc Boston 71-74.

Donaldson R J Jr, 1975 Preprints 16th Radar Meteor Conf Am Meteor Soc Boston 80-82.

Donaldson R J Jr, Dyer R M and Kraus M J, 1975 Air Force Surveys in Geophys No. 301 AFCRL-TR-75-0103 26 pp.

Eccles P J and Atlas D, 1973 J Appl Meteor, 12 847-854.

Eccles P J and Mueller E A, 1971 J Appl Meteor, 10 1252-1259.

Faller A J, 1965 J Atmos Sci, 22 176-184.

Fetter R W, 1970 Preprints 14th Radar Meteor Conf Am Meteor Soc Boston 413-418.

Frisch A S, Miller L J and Strauch R G, 1974 Geophys Res Letters, 1 86-69.

Frisch A S and Strauch R G, 1976 J Appl Meteor, 15 1012-1017.

Geotis S G, 1963 J Appl Meteor, 2 270-275.

Geotis S G, 1964 Proc 11th Weather Radar Conf Am Meteor Soc Boston 6-9.

Glover K M, Boucher R J, Ottersten H and Hardy K R, 1969 J Appl Meteor, 8 634-640.

Glover K M and Duquette E F, 1970 Preprints 14th Radar Meteor Conf Am Meteor Soc Boston 89-94.

Gray G R, Serafin R J, Atlas D, Rinehart R E and Boyajian J J, 1975 Bull Am Meteor Soc, 56 581-588.

Groginsky H L, 1965 Electron Prog (Raytheon Co) 9 (3) 7-13.

Gunn K and Marshall J S, 1958 J Meteor, 15 452-461.

Hardman M E, James D G and Goldsmith P, 1972 QJR Meteor Soc, 97 38-47.

Hardy K R, Atlas D and Browning K A, 1964 Proc 11th Weather Radar Conf Am Meteor Soc Boston 342-345.

Hardy K R, Atlas D and Glover K M, 1966 J Geophys Res, 71 1537-1552.

Hardy K R and Katz I, 1969 Atmospheric exploration by remote probes,2 (Washington DC: Nat Acad Sci) 217-243.

Hardy K R and Ottersten H, 1969 J Atmos Sci, 26 666-672.

Hardy K R, Reed R J and Mather G K, 1973 QJR Meteor Soc, 99 279-293.

Harper W G, 1957 QJR Meteor Soc, 83 368-371.

Harper W G, 1958 Proc Roy Soc B149 484-502.

Harper W G, 1960 Marine Observer, 30 36-40.

Harper W G, 1966 Meteor Mag, 95 106-112.

Harper W G, Ludlam F H and Saunders P M, 1957 Proc 6th Weather Radar Conf Am Meteor Soc Boston 267-273.

Harris F I, 1975 a Tech Report No. 35 Laboratory for Atmos Probing Univ of Chicago Dept of Geophys Sci.

Harris F I, 1975 b Preprints 16th Radar Meteor Conf Am Meteor Soc Boston 225-230.

Harrold T W, 1965 Sci Paper No. 21, Meteor Office (London : HMSO).

Harrold T W, 1967 Proc Inst Elect Eng, 114 201-203.

Harrold T W, 1973 QJR Meteor Soc, 99 232-251.

Harrold T W, 1975 Paper No. 8 Symposium on Weather Radar and Water Management, Published by Water Research Centre.

Harrold T W and Austin P M, 1974 J Rech Atmos, 8 41-57.

Harrold T W and Browning K A, 1967 Meteor Mag, 96 367-376.

Harrold T W and Browning K A, 1971 QJR Meteor Soc, 97 330-339.

Harrold T W, English E J and Nicholass C A, 1974 QJR Meteor Soc 100 331-350.

Harrold T W and Kitchingman P G, 1975 Preprints 16th Radar Meteor Conf Am Meteor Soc Boston 473-478.

Harrold T W and Nicholass C A, 1972 Meteor Mag, 101, 193-205.

Hicks J J and Angell J K, 1968 J Appl Meteor, 7 114-121.

Hildebrand P H, 1975 Preprints 16th Radar Meteor Conf Am Meteor Soc Boston 231-236.

Hill F F, Whyte K W and Browning K A, 1977 Meteor Mag, 106 69-89.

Hilst G R and Russo J A Jr, 1960 Tech Memo No. 3 Contract AF30-635-14459 The Travellers Weather Res Centre Inc

Hitschfeld W and Bordan J, 1954 J Meteor, 11 58-67.

Hitschfeld W and Dennis A S, 1956 Sci Report MW-23 Montreal : Stormy Weather Group, McGill Univ.

Houze R A Jr, Hobbs P V, Biswas K R and Davis W M, 1976 Mon Weather Rev, 104 868-878.

Houze R A Jr, Locatelli J D and Hobbs P V, 1976 J Atmos Sci, 33 1921-1936.

Humphries R G, 1974 Scientific Report MW-82 Stormy Weather Group, McGill Univ Montreal 81 pp.

Imai J, 1960 Proc 8th Weather Radar Conf Am Meteor Soc. Boston 211-218.

James P K and Browning K A, 1978 To be published.

Jameson A R, 1975 Preprints 16th Radar Meteor Conf Am Meteor Soc Boston 43-48.

Jatila E, 1973 Geophysica, 12 1-10.

Johnson D S, 1973 World Meteor Org Pub No. 342 11-31.

Johnson G N, Smith P L Jr, Nathanson F E and Brooks L W, 1975 Report prepared for NOAA, National Weather Service, Silver Spring, Md Contract No. 4-35341. Inst of Atmos Sci, South Dakota Sch of Mines and Tech Report No. 75-2.

Joss J, Schram K, Thams J C and Waldvogel A, 1970 On the quantitative determination of precipitation by radar. Wissenschaftliche Mitteiling Nr 63 Zurich : Eidgenössische kommission zum studium der Hagelbildung und der Hagelabwehr.

Joss J and Waldvogel A, 1970 Preprints 14th Radar Meteor Conf Am Meteor Soc, Boston 153-156.

Kessler E, 1961 Proc 9th Weather Radar Conf Am Meteor Soc, Boston 13-36.

Kessler E, 1968 Radar Measurement of Precipitation for Hydrological Purposes, Rept No. 5 (Geneva : World Meteor Org) 1-29.

Konrad T G, 1970 J Atmos Sci, 27 1138-1147.

Kropfli R A and Miller L J, 1976 J Atmos, Sci, 33 520-529.

Lane J A, 1969 Proc IEE, 116 1656-1660.

Lane J A and Meadows R W, 1963 Nature, 197 35-36.

Leach W, 1957 Proc 6th Weather Radar Conf Am Meteor Soc, Boston 151-156.

Lhermitte R M, 1963 Proc 10th Weather Radar Conf Am Meteor Soc, Boston, 323-329.

Lhermitte R M, 1964 Bull Am Meteor Soc, 45 587-596.

Lhermitte R M, 1966a Bull Am Meteor Soc, 47 703-711.

Lhermitte R M, 1966b J Atmos Sci, 23 575-591.

Lhermitte R M, 1968a Proc 13th Radar Meteor Conf Am Meteor Soc, Boston 498-503.

Lhermitte R M, 1968b Proc 13th Radar Meteor Conf Am Meteor Soc, Boston 14-17.

Lhermitte R M, 1969 Atmospheric Exploration by Remote Probes, 2 253-285 (Washington DC : Nat Acad Sci).

Lhermitte R M and Atlas D 1961 Proc 9th Weather Radar Conf Am Meteor Soc, Boston 218-223.

Lhermitte R M and Miller L J, 1970 Preprints 14th Radar Meteor Conf Am Meteor Conf Boston 133-138.

Ligda M G H, 1957 Tech Report No. X, Dept of Ocean and Meteor, A and M College of Texas.

Ligda M G H and Bigler S G, 1958 J Meteor, 15 494-501.

Locatelli J D and Hobbs P V, 1974 J Geophys Res, 79 2185-2197.

Luckenback G, 1958 Proc 7th Weather Radar Conf Am Meteor Soc, Boston D41-47.

McGrew R G, 1972 Preprints 15th Radar Meteor Conf Am Meteor Soc, Boston 101-106.

Marshall J S, 1953 J Meteor, 10 25-29.

Marshall J S, 1957 Proc 6th Weather Radar Conf Am Meteor Soc, Boston 321-324.

Marshall J S and Hitschfeld W, 1953 Canadian J Phys, 31 962-994.

Marshall J S and Palmer W M K, 1948 J Meteor, 5 165-166.

Marwitz J D, 1973 J Appl Meteor, 12 1174-1182.

Mason B J, 1973 Phys in Tech, 4, 62-75

Maynard R H, 1945 J Meteor, 2, 214-226.

Mel'nichuk Y V, 1971 Radar Meteorology Proc 3rd All-Union Conf (Jerusalem : Israel Program for Scientific Translations) 132-141.

Miles J W and Howard L N, 1964 J Fluid Mech, 20 331-336

Miller L J, 1972 Preprints 15th Radar Meteor Conf Am Meteor Soc Boston, 309-314

Miller L J, 1975 Pure and Appl Geophys, 113 765-785

Miller L J, and Strauch R G, 1974 Remote Sensing of Environ, 3, 219-235.

Moore P L and Smith D L, 1972 J Appl Meteor, 11, 1293-1298.

Nash J and Browning K A, 1978 To be published.

Nathanson F E, 1969 Radar Design Principles (New York; McGraw-Hill).

Newell R E, 1958 Proc 7th Weather Radar Conf, Am Meteor Soc Boston E50-E56.

Nicholass C A and Harrold T W, 1975 Meteor Mag, 104, 208-216.

Noonkester V R, 1974 Naval Elec Lab Center Tech Rept 1919 San Diego California 70 pp.

Nozumi Y and Arakawa H, 1967 J Geophys Res, 73, 487-492.

Ohtake T and Henmi T, 1970 Preprints 14th Radar Meteor Conf Am Meteor Soc Boston 209-210.

Orlanski I, 1975 Bull Am Meteor Soc, 56, 527-530.

Ottersten H, 1970 Preprints 14th Radar Meteor Conf Am Meteor Soc Boston, 111-116.

Peck E L, Larson L W and Wilson J W, 1973 In Advanced Concepts in the Study of Snow and Ice Resources, Nat Acad Sci Washington DC 412-421.

Pollock D M and Wilson J W, 1972 IFYGL Tech Plan Vol 1 107-112.

Probert-Jones J R, 1962 QJR Meteor Soc, 88, 485-495.

Probert-Jones J R, and Harper W G, 1961 Proc 9th Weather Radar Conf Am Meteor Soc Boston 225-232.

Ramage C S, 1976 Bull Am Meteor Soc, 57 4-10

Ray P S, Doviak R J, Walker G B, Sirmans D, Carter J and Bumgarner W C, 1975 J Appl Meteor, 14, 1521-1530.

Readings C J, Golton E and Browning K A, 1972 Boundary-layer Meteor 4 275-287.

Richter J H, 1969 Radio Sci, 4 1261-1268.

Roach W T, 1972 Clear Air Turbulence (Watford : Merrow).

Rogers R R, 1964 Proc 11th Weather Radar Conf Am Meteor Soc Boston 158-160.

Rogers R R, 1967 Tellus, 19, 432-455.

Rogers R R and Tripp B R, 1964 J Appl Meteor, 3, 603-610.

Rummler W D, 1968 Tech Memo MM-68-4121-5 Bell Tel Labs Whippany, New Jersey, 28 pp.

Ryde J W, 1947 Meteor Factors in Radio Wave Propagation, Phys, Soc 169-189.

Scofield R A and Weiss C E, 1976 Preprints 6th Conf Weather Forecasting and Analysis Am Meteor Soc Boston, 67-73.

Simpson J E, Mansfield D A and Milford J R, 1977 QJR Meteor Soc 103 47-76.

Sirmans D and Bumgarner W C, 1975 J Appl Meteor, 14 991-1003.

Sirmans D and Doviak R J, 1973 J Appl Meteor, 12 694-697.

Sirmans D, Doviak R J, Burgess D and Lemon L R, 1974 Bull Am Meteor Soc, 55 1126-1127.

Sirmans D, Zrnic D and Bumgarner W C, 1976 Preprints 17th Radar Meteor Conf Am Meteor Soc Boston 23-28.

Skolnik M I, 1962 Introduction to Radar Systems. (New York : McGraw Hill).

Smith P L and Rogers R R, 1963 Proc 10th Weather Radar Conf Am Meteor Soc Boston, 316-322.

Smith R L and Holmes D W, 1961 Mon Weather Rev, 89 1-7.

Srivastava R C and Jameson A R, 1975 National Hail Research Experiment Symposium/Workshop on Hail Estes Park, Colorado Preprint Vol 1 pp VIIICa1-25.

Stackpole J D, 1961 Proc 9th Weather Radar Conf Am Meteor Soc Boston 212-217.

Starr J R and Browning K A, 1972 QJR Meteor Soc, 98 73-85.

Stout G E and Huff F A, 1953 Bull Am Meteor Soc, 34 281-284.

Stout G E and Mueller E A, 1968 J Appl Meteor, 7 465-474.

Strauch R G, Campbell W C, Chadwick R B and Moran K P, 1976 Geophys. Res. Letters, 3 193-196.

Sulakvelidze G K, Bibilashvili N Sh and Lapcheva V F, 1967 Formation of Precipitation and Modification of Hail Processes (Jerusalem : Israel Program for Scientific Translations).

Tatarski V I, 1961 Wave Propagation in a Turbulent Medium (New York : McGraw Hill).

Taylor B C and Browning K A, 1974 Weather, 29 202-216.

Vonnegut B and Moore C B, 1958 Giant electrical storms, Recent Advances in Atmos Electricity, Ed L G Smith, (New York : Pergamon Press) 399-411.

Wallace P R, 1953 Canadian J Phys, 31 995-1009.

Water Resources Board, 1973 Report by the Operations Systems Group (Water Resources Board, Reading).

Watkins C D, 1971 Proc IEE, 118 519-528.

Watkins C D and Browning K A, 1973 Phys in Tech, 4 28-61.

Weible M L and Sirmans D, 1976 Preprints 17th Radar Meteor Conf Am Meteor Soc Boston 75-78.

Weiss R R, Locatelli J D and Hobbs P V, 1976 Preprints 17th Radar Meteor Conf Am Meteor Soc Boston 226-227.

Wexler R and Atlas D, 1963 J Appl Meteor, 2 276-280.

Wilson D A, 1970 Preprints 14th Radar Meteor Conf Am Meteor Soc Boston 191-196.

Wilson J W, 1966 Tech Memo 28 Nat'l Severe Storms Lab Norman Oklahoma.

Wilson J W, 1970 J Appl Meteor, 9 489-497.

Wilson J W, 1975 Final Report to the Great Lakes Environmental Research Lab, NOAA. The Center for the Environment and Man Inc Report 4177-540.

Woodley W L, Olsen A R, Herndon A and Wiggert V, 1975 J Appl Meteor, 14 909-928.

Woodroffe A, 1976 World Met Org No. 450 (Papers presented at the WMO Symposium on the Interpretation of Broad-scale NWP Products for Local Forecasting purposes) 170-175.

Woods J D, 1968 J Fluid Mech, 32 791-800.

World Meteorological Organization, 1966 Tech Note No. 78 (Geneva : Secretariat of the World Meteor Org).

Zrnic D S and Doviak R J, 1975 J Appl Meteor, 14 1531-1539.

LIST OF CAPTIONS

Fig 1 Geometry of a radar pulse volume.

Fig 2 Mean error (without regard to sign) in the measurement of areal rainfall, using a radar calibrated against a single raingauge, plotted as a function of the area and period of integration (From Collier 1977).

Fig 3 Mean error of the hourly rainfall totals in subcatchments of average area 60 km^2, as determined from radar measurements in various kinds of rainfall conditions, plotted as a function of the number density of calibrating raingauge sites (solid curves). Also shown for comparison is the mean error of the hourly subcatchment totals as determined from a network of raingauges in the absence of radar, again plotted as a function of the number density of raingauge sites (dotted curves). The set of four dotted curves represents the measurement errors for the raingauge network in the presence of (1) extremely isolated showers, (2) typical showers, (3) typical widespread rain, and (4) extremely uniform rain. For all curves the mean error is defined as the mean value of the difference between the estimated rainfall and the 'optimum estimate' (defined in the text) without regard to sign. (After Collier 1977).

Fig 4 Schematic illustration of the dual wavelength method of hail detection proposed by Eccles and Atlas. (From Carbone et al 1973).

Fig 5 Observed depolarization and reflectivities in Alberta thunderstorms. Estimates of hail size are based upon ground observation. Very small hail (h) corresponds here to hail with diameter less than 5 mm. Figure prepared by Srivastava and Jameson (1975) from data in Barge (1972) and Humphries (1974).

Fig 6 (a and b) Photographs of the PPI display showing (a) uniform warm frontal rain on 19 November 1972 and (b) widespread showers on 23 May 1974, as seen by a 10 cm radar at Malvern. Only half the display is shown since the radar is blocked by hills to the west. Range markers are at 18 km (10 naut mi) intervals. The east coast of England is outlined.

Fig 6 (c) Photograph of the RHI display taken during a situation on 12 November 1972 resembling that in Fig 6(a), as seen by a mobile Malvern 10 cm radar located in South Wales. The two shades of grey are set to represent echo intensities 5 dB apart so as to depict the bright band echo at a height of about 1 km.

Fig 7 Photographs of the PPI display showing examples of different types of precipitation bands encountered in the British Isles. (a) shows a pre-cold frontal convective rainband on 5 December 1972, (b) shows a uniform post cold frontal rainband on 12 November 1970 and (c) shows shallow line convective at the surface cold front on 11 November 1970. (a) and (b) were obtained from a 10 cm radar at Malvern; range markers are at 18 km (10 naut mi) intervals. (c) was obtained from a mobile Malvern 10 cm radar sited on the Isles of Scilly; the main range marker is at 50 km.

Fig 8 Photographs of the THI display (a and b) and the RHI display (c) showing different kinds of non-precipitating cloud as seen by an 8.6 mm radar at Malvern. (a) shows altocumulus cloud at an altitude of 2 km on 18 September 1962 and (b) shows thick altostratus on 13 August 1962 (both from Harper 1966) . (c) shows thick altostratus with stalactites at cloud base as seen on 9 November 1972.

Fig 9 Photograph of the RHI display showing a severe local storm with tops to 12.8 km, as seen by a 3 cm radar at Malvern on 13 July 1967. This storm gave damaging winds and hail with diameter exceeding 5 cm. The weaker storm cells with tops around 6 km gave only rain. Range markers are at intervals of about 18 km (10 naut mi); height markers are at intervals of about 3 km (10,000 ft).

Fig 10 Photograph of the PPI display showing the hook echo associated with the tornado which struck Meriden on 19 May 1960, as seen by a 10 cm radar at Topeka, Kansas. Range markers are at intervals of 9 km (5 naut mi). (Photograph from the US National Oceanic and Atmospheric Administration).

Fig 11 Photograph of the PPI display showing the spiral rainbands associated with Hurricane Debra as seen by a 3 cm radar in Texas. Range markers are at intervals of 40 km (25 stat mi). The hurricane eye is at 200 km, 143 deg. (From Hardy et al 1964).

Fig 12 Photograph of the RHI display showing a severe local storm with a weak-echo vault indicative of an intense updraught as seen by a 10 cm radar near Oklahoma city. Range markers are at intervals of about 18 km (10 naut mi); height markers are at intervals of about 3 km (10,000 ft). (From Browning 1965).

Fig 13 Lineprinter output of the data from a 5.6 cm radar at Llandegla in North Wales (*) as it was received at Malvern within a minute of real time. Two major rainbands can be seen oriented roughly north-south across northwest England and the West Midlands. The numerals 1 to 5 represent rainfall intensities averaged over 5 km squares of 0.2, 0.4, 0.8, 1.6 and 3.2 mm h^{-1}. Coastlines are shown dotted. Time (1703) is shown in the top left corner. The date, 9 June 1976, is in the top right corner. Figures at the foot of the print-out represent hourly rainfall totals in a number of river subcatchments.

Fig 14 Schematic diagram illustrating how vertical air velocity can be estimated from the Doppler spectrum with the radar beam pointing vertically in precipitation. Z is the reflectivity factor and V_r is the Doppler velocity. Curve I is the Doppler spectrum owing to the terminal fallspeed V_f of the precipitation alone, curve II is the spectrum owing to the terminal fallspeed plus an updraught, and curve III is the same as curve II plus the effect of turbulence. (From Browning 1971 a).

Fig 15 Time-height section showing vertical air velocity in a shower cloud as derived using (a) the lower-bound method and (b) Rogers' method. Isotachs are at intervals of 2 m s^{-1}; regions of downward velocity are stippled. (From Battan and Theiss 1970).

Fig 16 Illustration of the principle of the conical scanning technique with examples of actual results. (From Lhermitte 1969).

Fig 17 Air motion associated with a cold front as derived from Doppler radar measurements made near Malvern. (a) and (b) illustrate the pattern of air motion within vertical sections; (a) depicts the broad pattern of airflow, derived from a sequence of conical scans, and (b) depicts the detailed airflow at the surface cold front within part of the area covered by (a), as derived from RHV scans. Solid curves are streamlines, dashed curves are isopleths of vertical velocity and the hatched shading in (b) denotes the cold frontal zone. The photograph in (c) shows part of the range-velocity display of the Doppler radar when it was scanning through the sharp wind shift at the surface cold front. (After Browning and Harrold 1970).

Fig 18 Turbulent structure at the base of an altostratus cloud deck characterized by stalactites, observed by a Doppler radar at RSRE Defford. (a) shows the reflectivity factor in dBz and (b) shows the Doppler velocity with isotachs at 2 m s^{-1} intervals, as determined from RHV scans within a vertical section oriented into the wind. (After Harris 1975a).

Fig 19 Detailed airflow pattern, inferred from dual Doppler radar data, within a vertical section along the direction of travel of a hailstorm in northeast Colorado. Velocity vectors represent flow relative to the storm, the velocity scale being shown by the vertical 10 m s^{-1} vector. The solid contours represent radar reflectivity at 8 dB intervals. Approximate cloud outlines, gust front and inflow measurements from a low-flying aircraft have also been added

Fig 19 (contd) to provide context. The chain of large dots represents the computed trajectory of a growing hailstone. (Adapted by J C Fankhauser and I Paluch from Kropfli and Miller 1976).

Fig 20 A tornado vortex signature (TVS) as obtained from a single Doppler radar on the occasion of the destructive tornado which hit Union City, Oklahoma, on 24 May 1973. (a) shows isopleths of radar reflectivity (solid curves labelled in dBz) and also streamlines of the low level airflow (dashed lines) which are consistent with Doppler radar measurements made at 1545 CST. The location of the tornado is indicated by an asterisk. (b) is an enlargement of the dotted area in (a) and it shows values of mean Doppler velocity (labelled in m s^{-1}) within individual range gates spaced 600 m apart and at 1-deg intervals of azimuth (N = no data). The small rectangle enclosing adjacent velocity values of -30 and +23 m s^{-1} is indicative of a TVS. Note that it corresponds well with the location of the tornado at the ground as indicated by the asterisk. (Adapted from Burgess et al 1975).

Fig 21 Photograph of the RHI display of the high-power radar at RSRE Defford, obtained on 13 May 1971, showing multiple layer echoes associated with a stably stratified atmosphere. Slant range marks are shown at 5 and 10 km. Non-linearity in the range scale accounts for the downward curvature of echoes at close ranges. Stationary targets have been removed by coherent filtering. (From Browning 1972).

Fig 22 Sequence of 3 photographs of the RHI display of the high-power radar at RSRE Defford, obtained on 22 April 1970, showing stationary lee waves downwind of the hills of South Wales. The RHI sections were obtained at 6-min intervals looking into the wind along 250 deg. Below 3 km the echoes are from the clear air and they show a standing wave pattern with waves decreasing from a maximum crest-trough amplitude of 600 m over the hills at 70 km range to less than 200 m near the radar. Above 3 km the echoes are from streamers of ice crystals and recognizable features can be seen travelling toward the radar at almost 30 m s^{-1}. Between 0908 and 0914 GMT the streamer identified by an asterisk can be seen ascending from a trough to a crest in the lee wave pattern.

Fig 23 Photographs of PPI displays showing thin lines of echo associated with (a) the cold density current outflow from a cluster of thunderstorm cells in England (From Harper 1960) and (b) a cloud-free cold front in Texas (From Ligda and Bigler 1958).

Fig 24 Photograph of the RHI display of the high-power radar at RSRE Defford, obtained on 10 May 1971, showing inverted U-shaped echoes outlining the tops of a train of convective cells within the boundary layer

Fig 25 Photograph of the PPI display of the high-power 10 cm radar at Wallops Island, obtained with the beam at an elevation of 3 deg, showing characteristic doughnut-shaped echoes where the beam intersects the upper parts of inverted U-shaped convective cells. (From Hardy and Ottersten 1969).

Fig 26 Depth of the convective boundary layer as determined by the high-power radar at RSRE Defford at about midday on 10 June 1970. Notice that the area of deeper convection (ADC) shown in (b) coincides with the high land of the Cotswolds as shown in (a). Two hours later the boundary layer had deepened to 3 km over the Cotswolds and after a further two hours thunderstorms broke out. (After Harrold and Browning 1971).

Fig 27 Photographs of THI display, obtained simultaneously from two vertically pointing FMCW radars in the San Diego region of California on 22 April 1973, showing the development of convection as cold sea air travelled inland. (a) shows echoes from the top of the 200 m deep boundary layer as seen by a radar on the coast; (b) shows echoes from the top of the convectively disturbed boundary layer as seen by another radar about 5 km inland (note the different height scale). (From Noonkester 1974).

Fig 28 Photograph of the RHI display of the high-power radar at RSRE Defford, showing Kelvin-Helmholtz billows of large amplitude responsible for clear air turbulence at an altitude of 5 to 6 km. Echoes from the top of the convective boundary layer and from an overlying stable layer can be seen at 1 and 2 km, respectively. The two range rings are at 5 and 10 km. Side-lobe echoes from the ground, often a major problem with high-power radars, have been largely avoided by coherent filtering (From Browning 1971b).

Fig 1

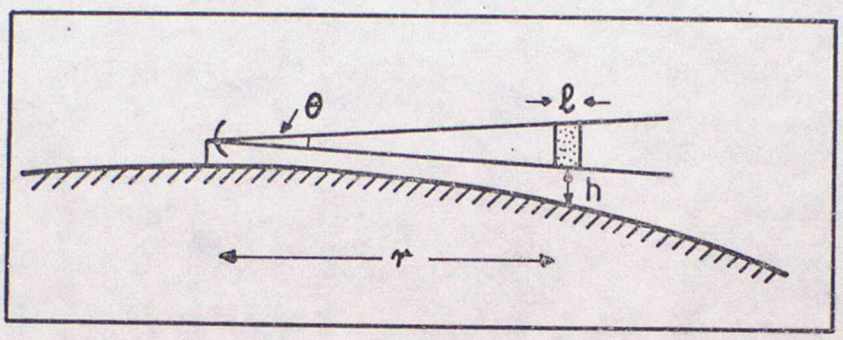
θ
ℓ
h
r

Fig 2

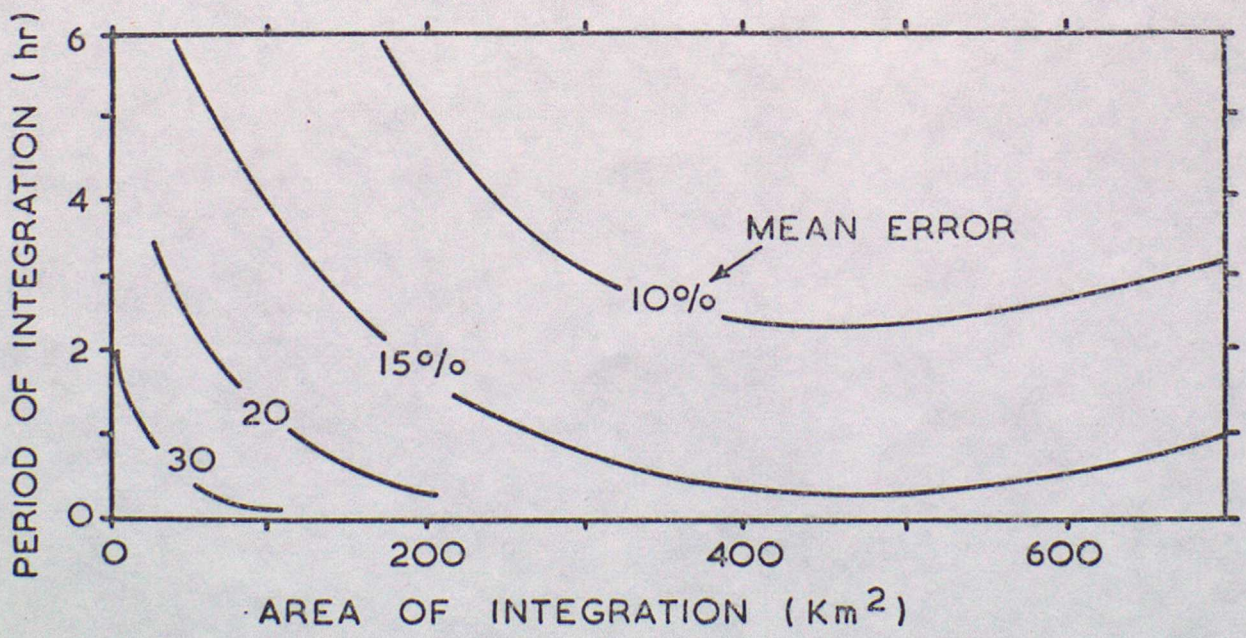
PERIOD OF INTEGRATION (hr)
6
4
2
0
0
200
400
600
AREA OF INTEGRATION (Km²)
MEAN ERROR
10%
15%
20
30

Fig 3

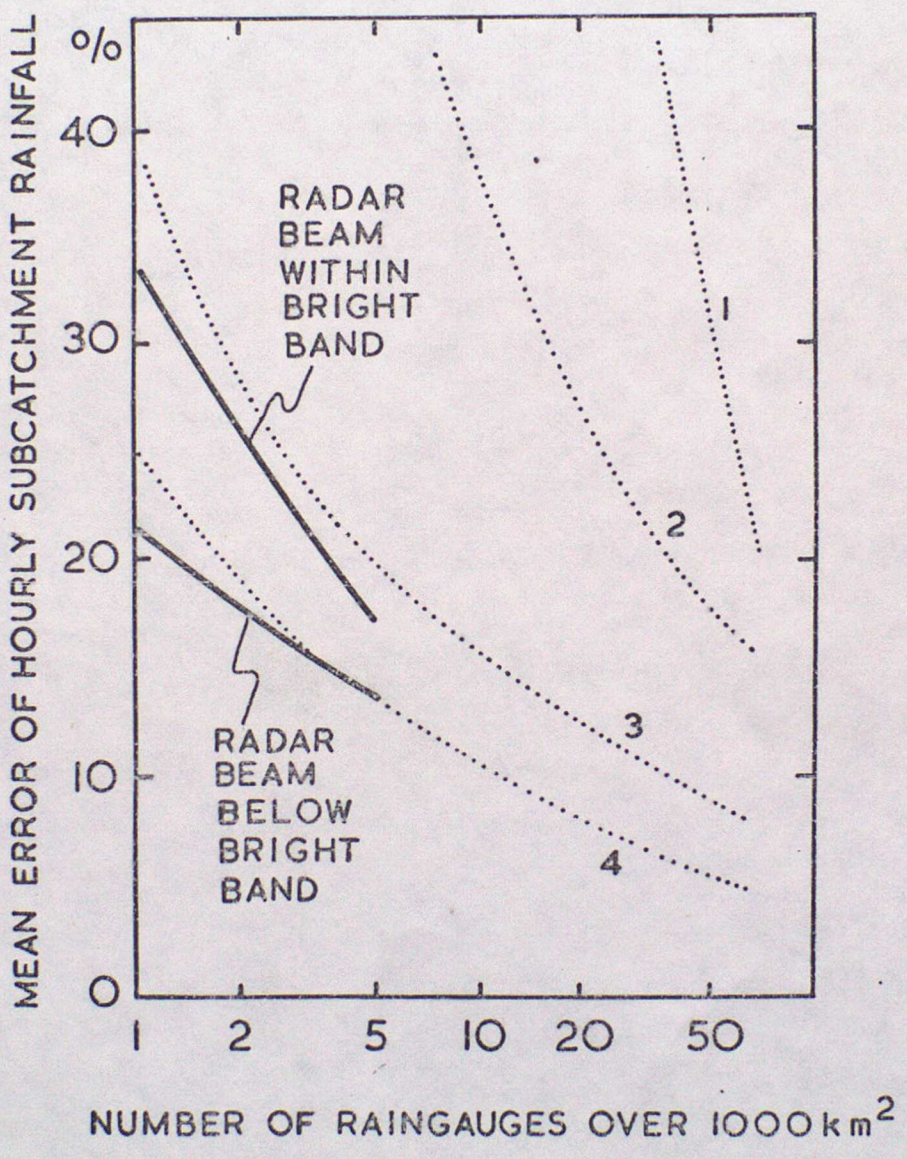
MEAN ERROR OF HOURLY SUBCATCHMENT RAINFALL
%
40
30
20
10
0
RADAR BEAM WITHIN BRIGHT BAND
RADAR BEAM BELOW BRIGHT BAND
1
2
3
4
1
2
5
10
20
50
NUMBER OF RAINGAUGES OVER 1000 km²

Fig. 4

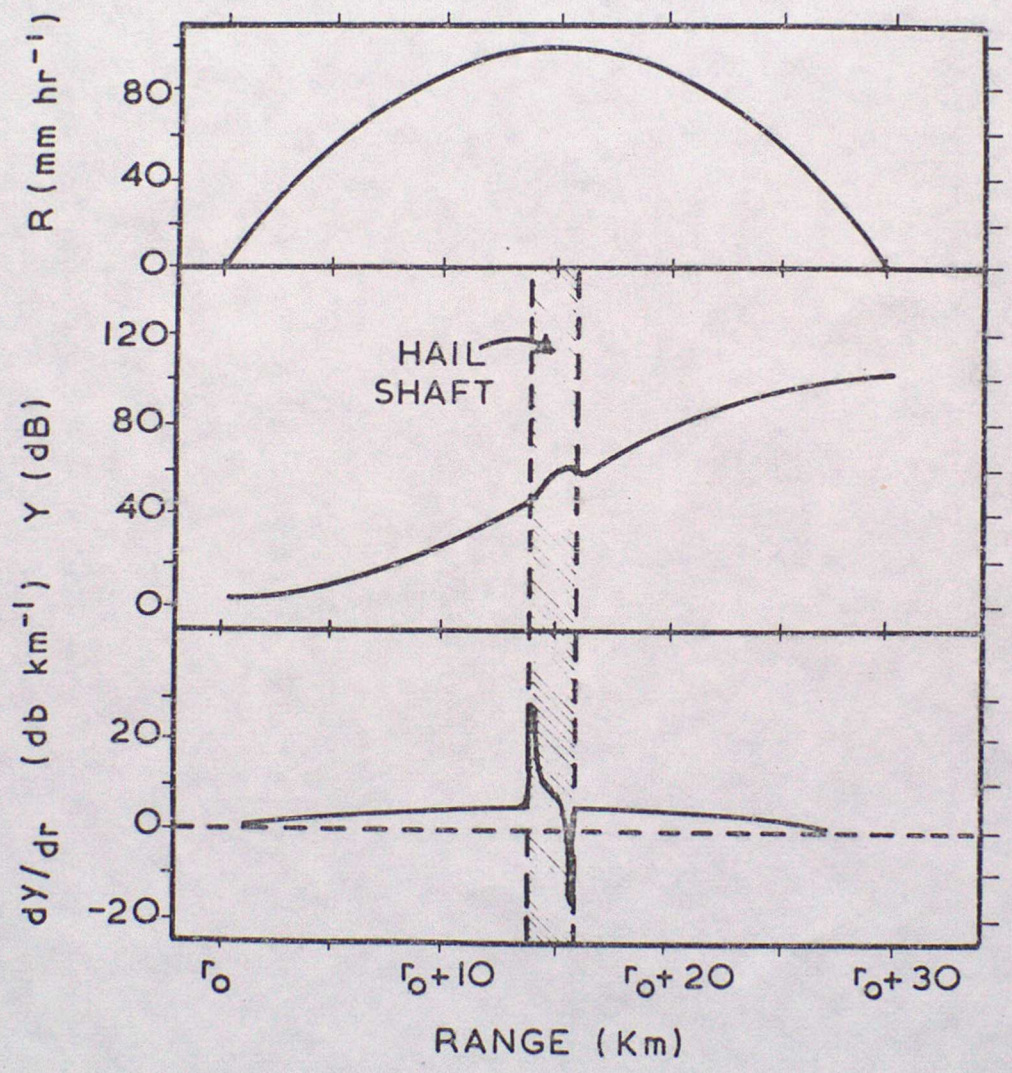
R (mm hr⁻¹)
80
40
0
120
80
40
0
Y (dB)
HAIL
SHAFT
dY/dr (db km⁻¹)
20
0
-20
r₀
r₀+10
r₀+20
r₀+30
RANGE (Km)

Fig. 5

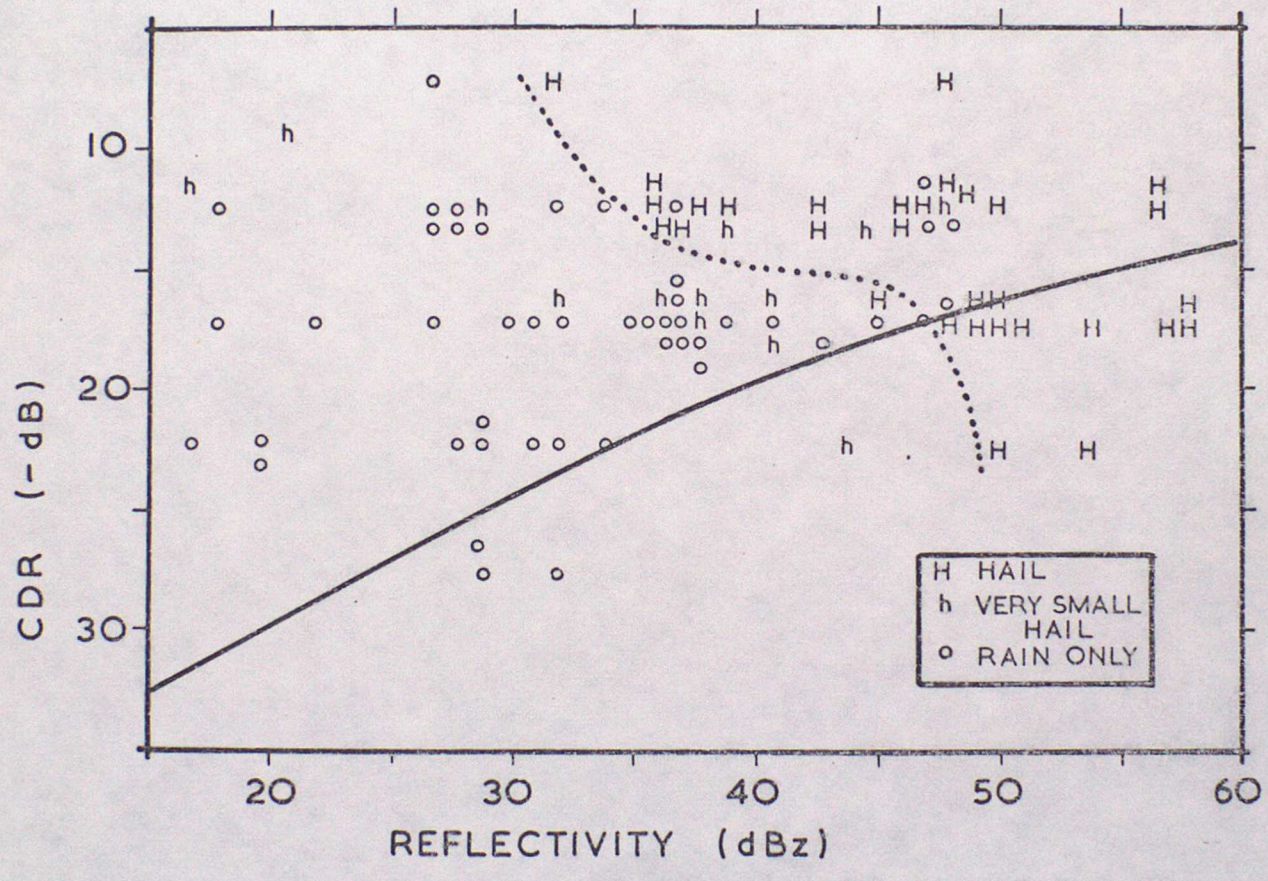
CDR (-dB)
10
20
30
20
30
40
50
60
REFLECTIVITY (dBz)
H HAIL
h VERY SMALL HAIL
o RAIN ONLY

Fig 6

(a)

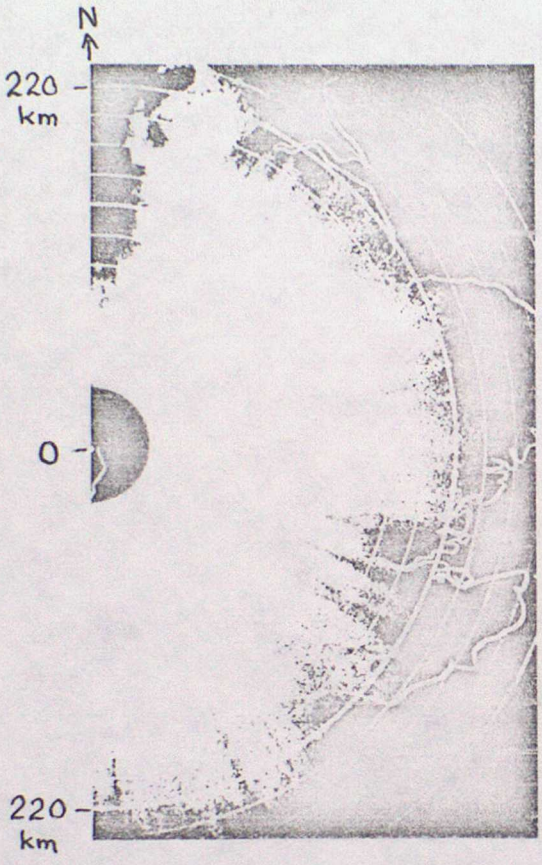

(b)

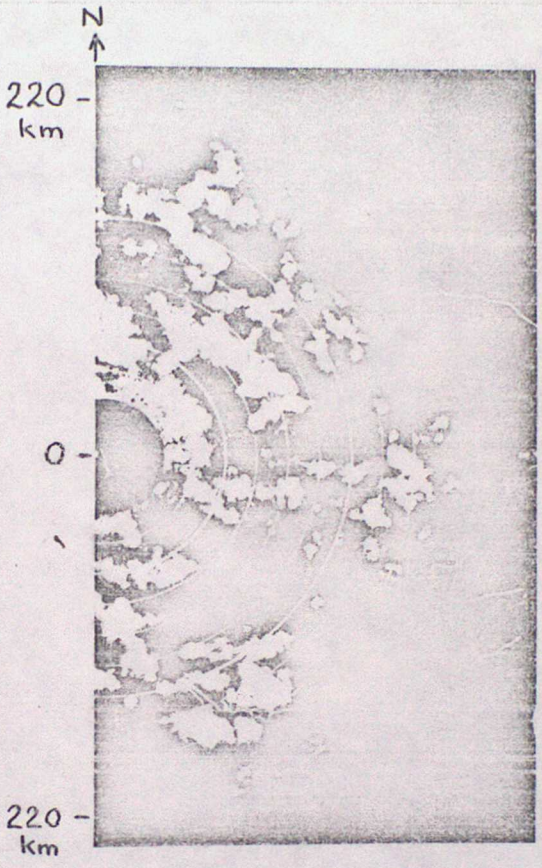

(c)

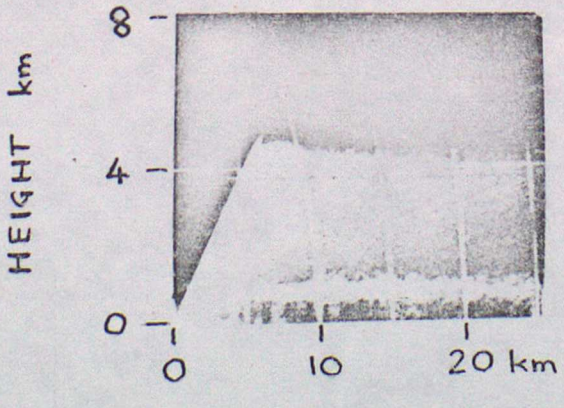

Fig 7

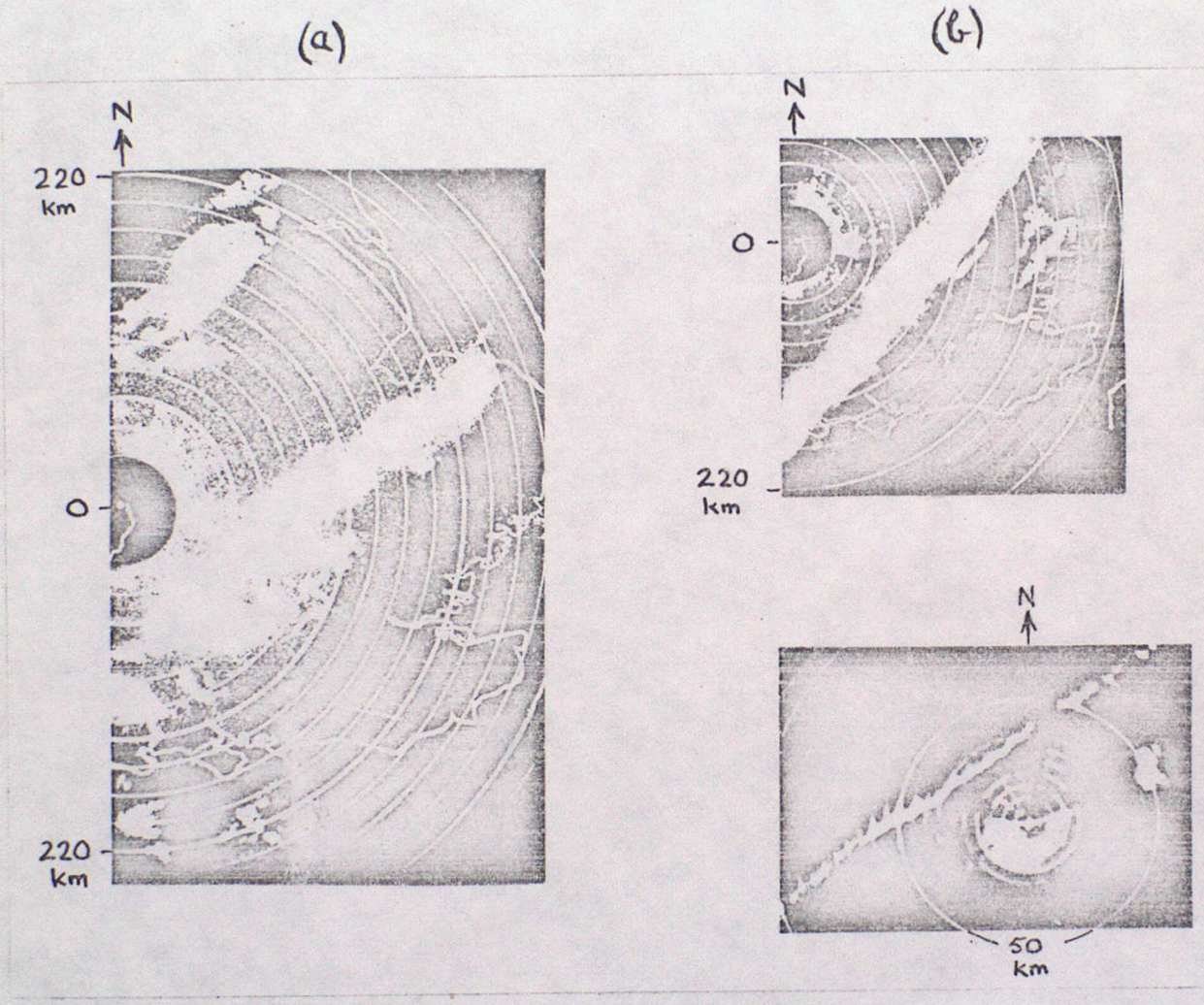

Fig 8

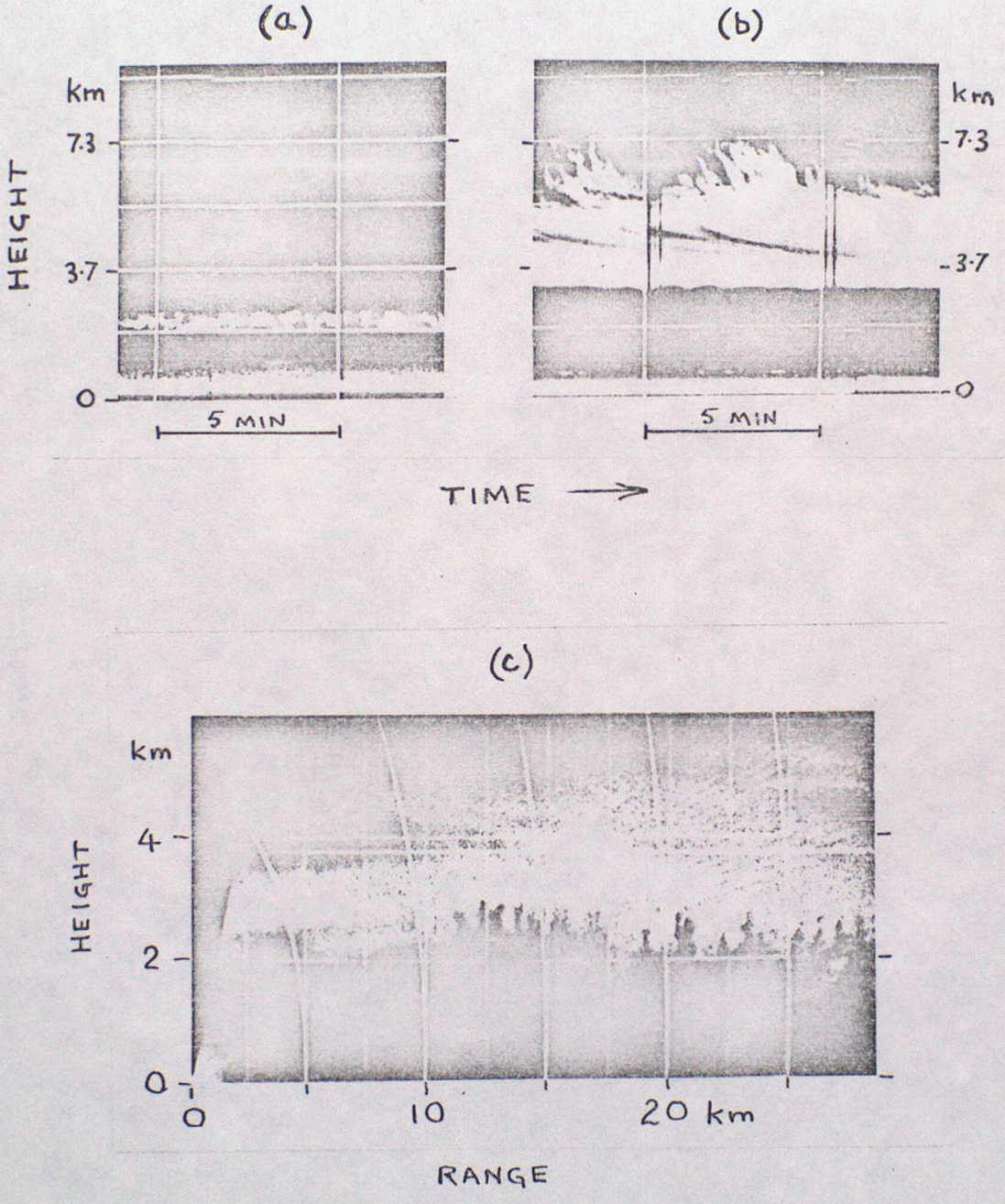
(a)
(b)
km
7·3
3·7
0
HEIGHT
5 MIN
5 MIN
TIME
(c)
km
4
2
0
HEIGHT
0
10
20 km
RANGE

Fig. 9

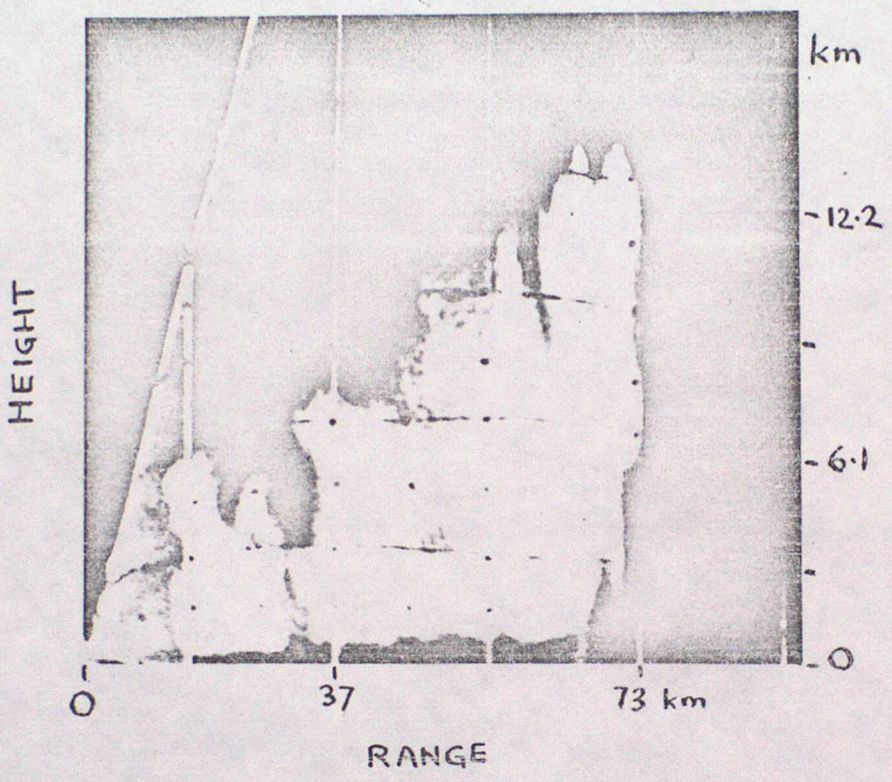

Fig 10

10 km

Fig 11.

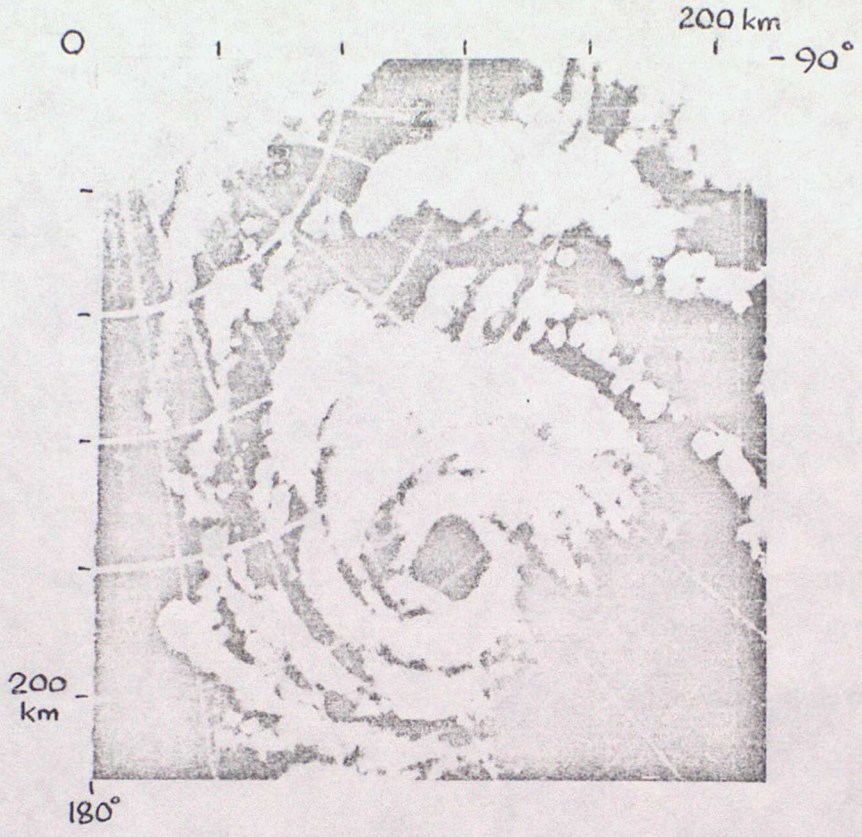

Fig 12

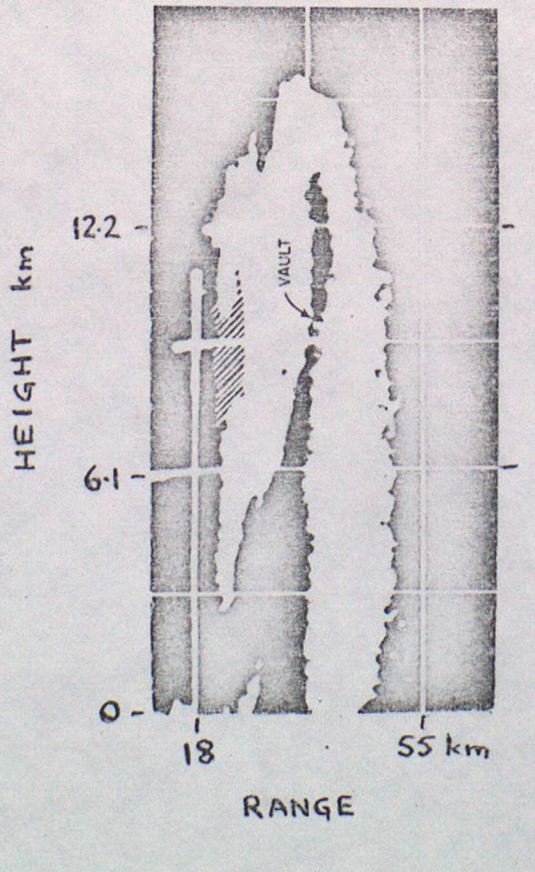

Fig 13

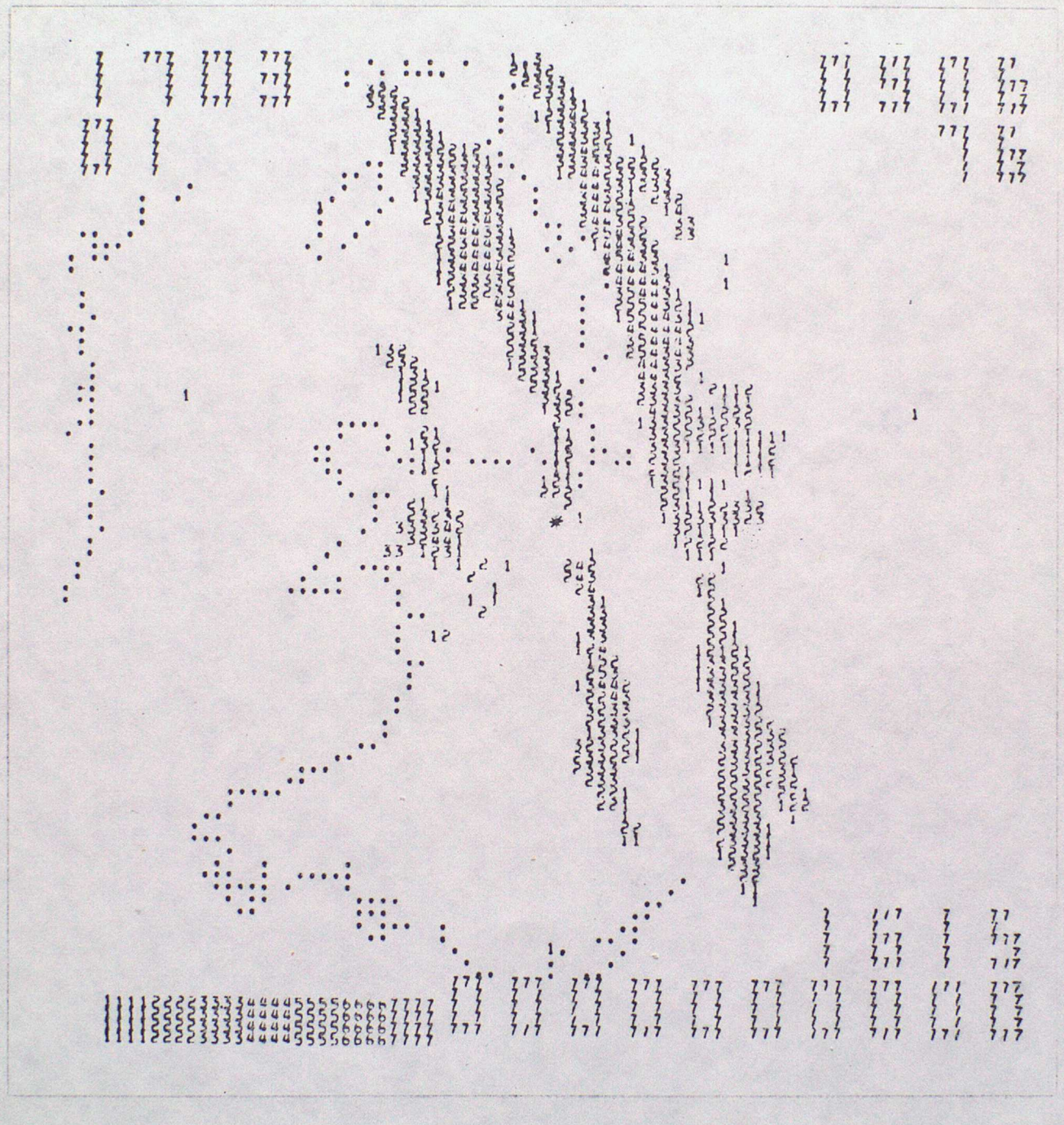

Fig 14

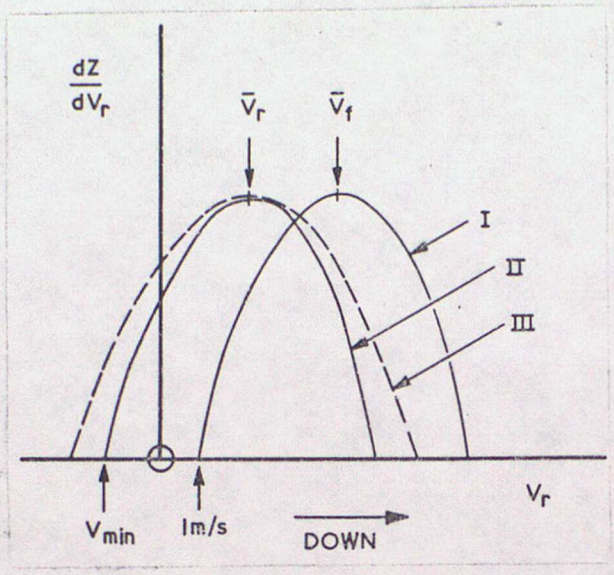
dZ/dVr
V̄r
V̄f
I
II
III
Vr
Vmin
1m/s
DOWN

Fig 15

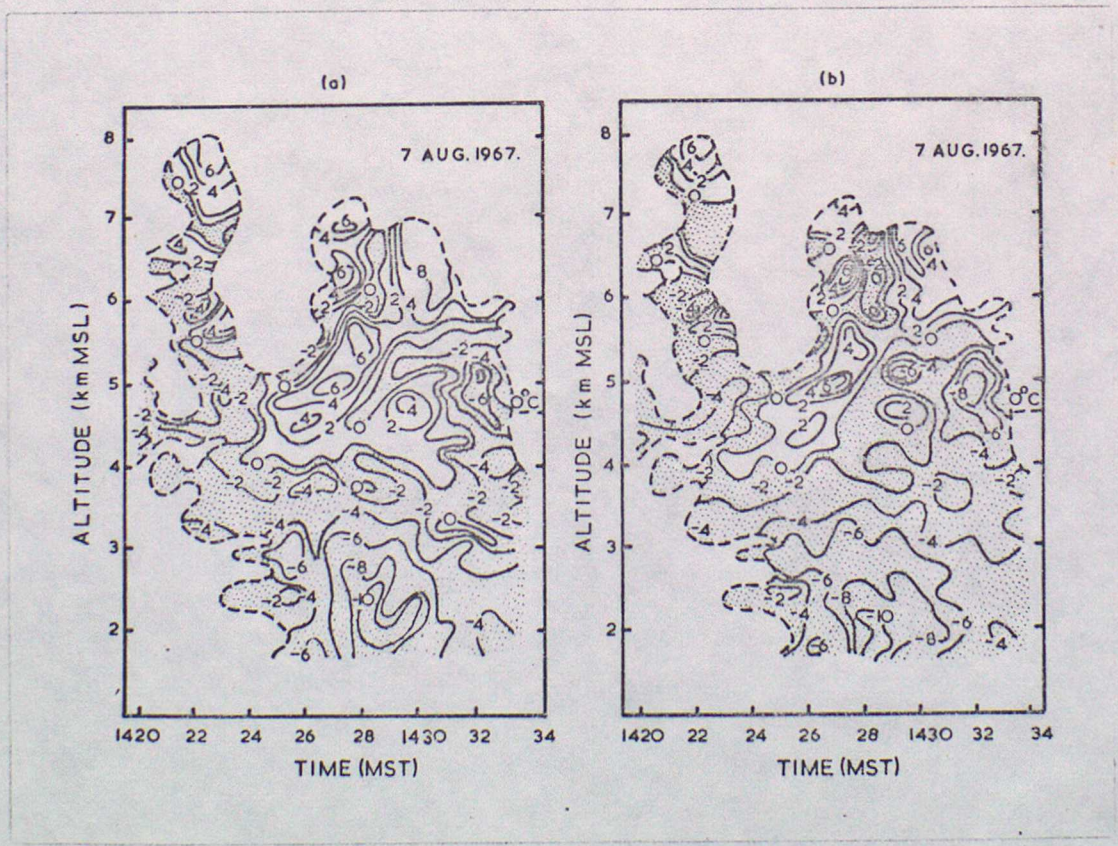
(a)
(b)
7 AUG. 1967.
7 AUG. 1967.
ALTITUDE (km MSL)
ALTITUDE (km MSL)
TIME (MST)
TIME (MST)
1420 22 24 26 28 1430 32 34
1420 22 24 26 28 1430 32 34

Fig 16

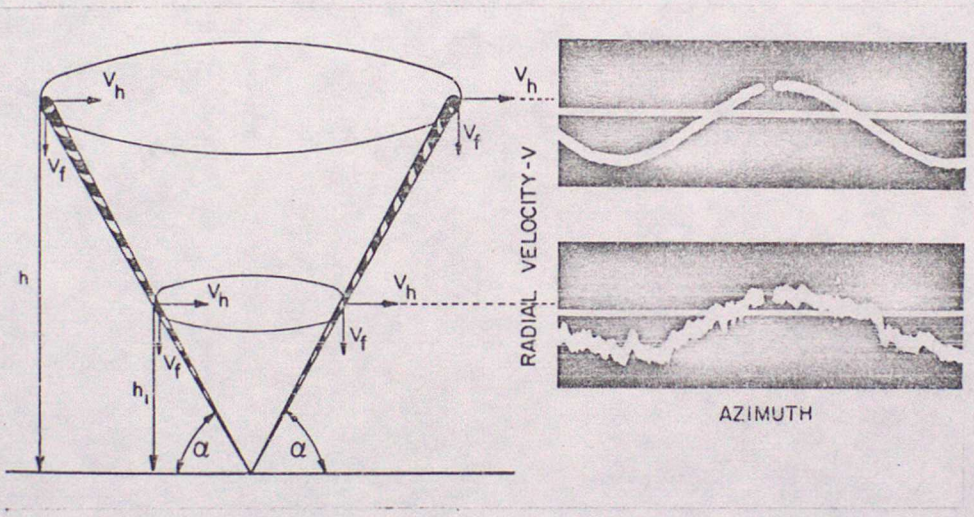

Fig. 17

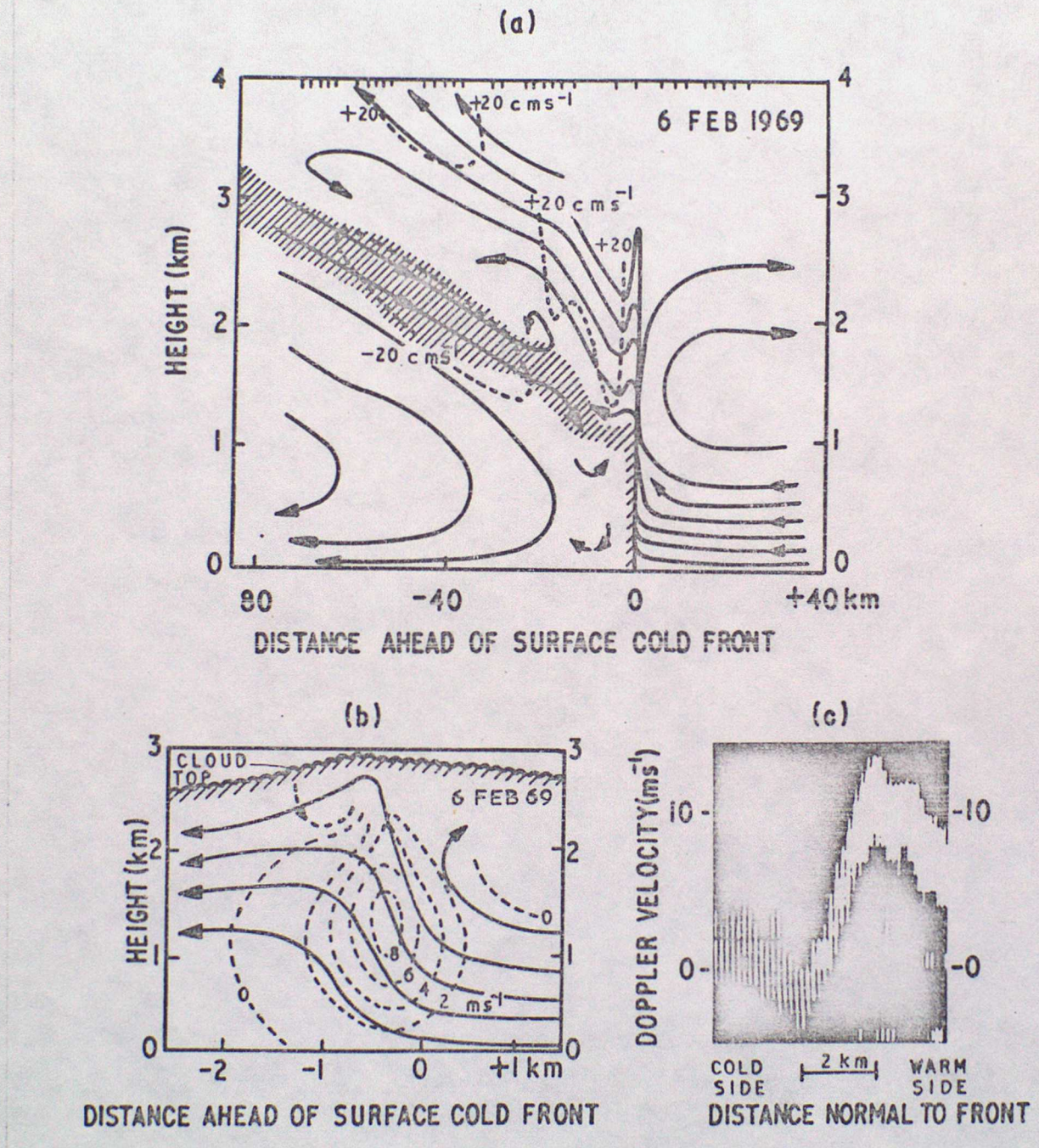
(a)
6 FEB 1969
+20 cms⁻¹
+20 cms⁻¹
+20 cms⁻¹
+20
-20 cms⁻¹
HEIGHT (km)
4
3
2
1
0
80
-40
0
+40 km
DISTANCE AHEAD OF SURFACE COLD FRONT
(b)
CLOUD TOP
6 FEB 69
HEIGHT (km)
0
-8
-6
-4
-2
ms⁻¹
-2
-1
0
+1 km
DISTANCE AHEAD OF SURFACE COLD FRONT
(c)
DOPPLER VELOCITY (ms⁻¹)
10
0
-10
-0
COLD SIDE
2 km
WARM SIDE
DISTANCE NORMAL TO FRONT

Fig 18

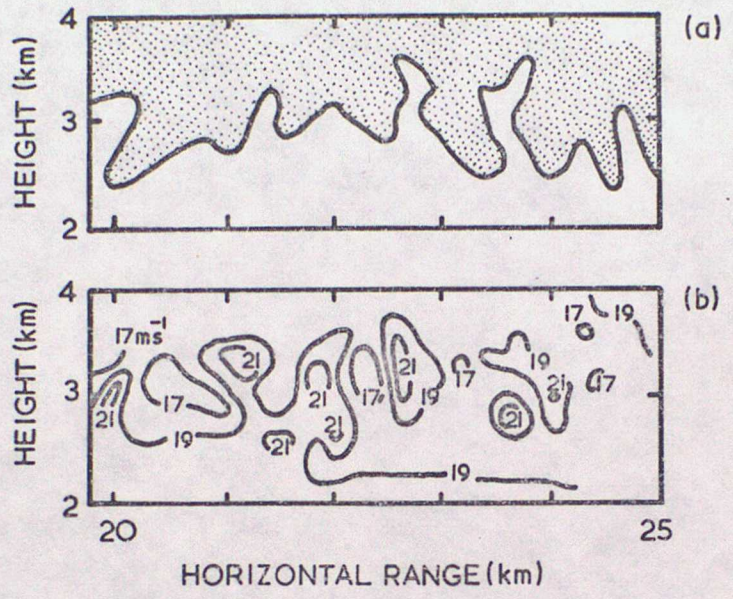
(a)
(b)
HEIGHT (km)
4
3
2
17ms⁻¹
21
17
19
20
25
HORIZONTAL RANGE (km)

Fig 19

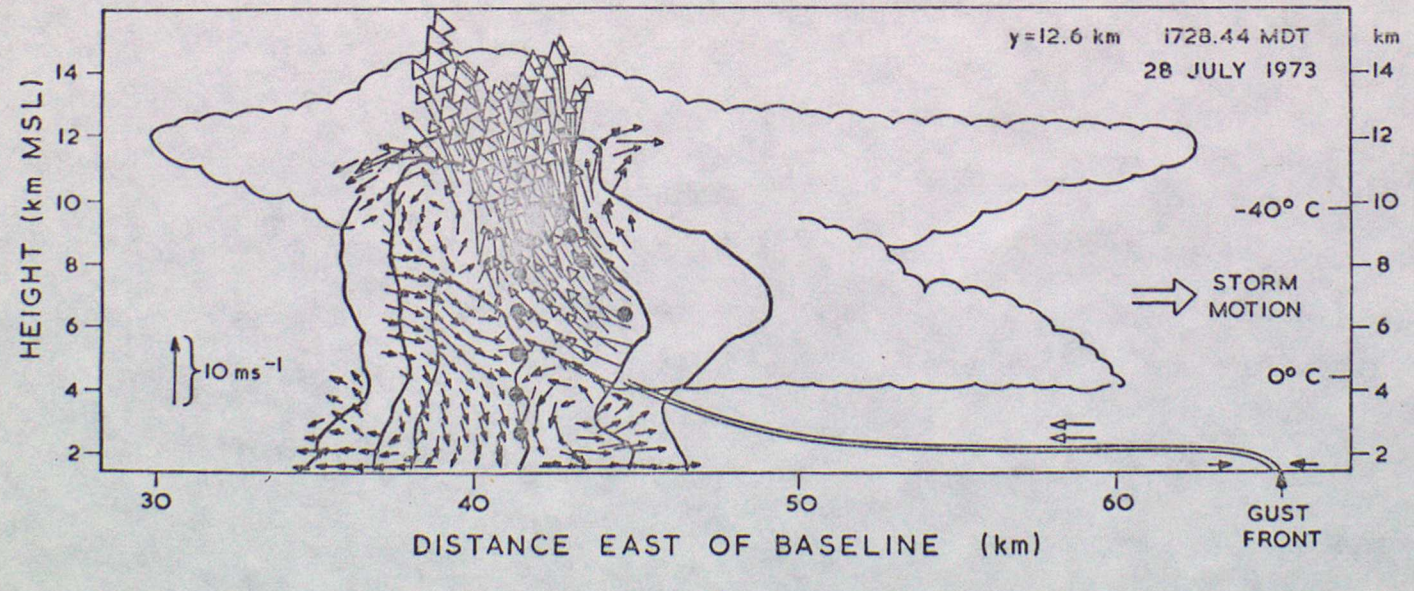
y=12.6 km
1728.44 MDT
28 JULY 1973
km
HEIGHT (km MSL)
14
12
10
8
6
4
2
-40° C
0° C
STORM MOTION
10 ms⁻¹
30
40
50
60
GUST FRONT
DISTANCE EAST OF BASELINE (km)

Fig 20

(a)

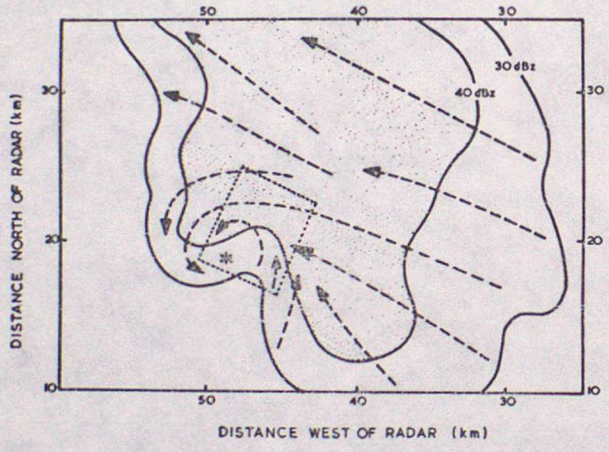
50
40
30
30 dBz
40 dBz
30
20
10
DISTANCE NORTH OF RADAR (km)
DISTANCE WEST OF RADAR (km)

(b)

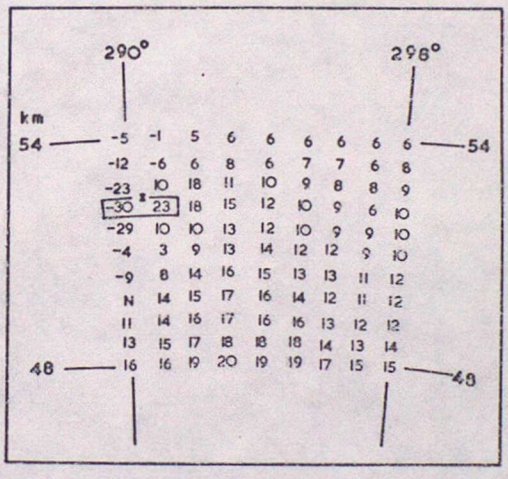
290°
298°
km
54
48
-5 -1 5 6 6 6 6 6 6
-12 -6 6 8 6 7 7 6 8
-23 10 18 11 10 9 8 8 9
-30 23 18 15 12 10 9 6 10
-29 10 10 13 12 10 9 9 10
-4 3 9 13 14 12 12 9 10
-9 8 14 16 15 13 13 11 12
N 14 15 17 16 14 12 11 12
11 14 16 17 16 16 13 12 12
13 15 17 18 18 18 14 13 14
16 16 19 20 19 19 17 15 15

Fig 21

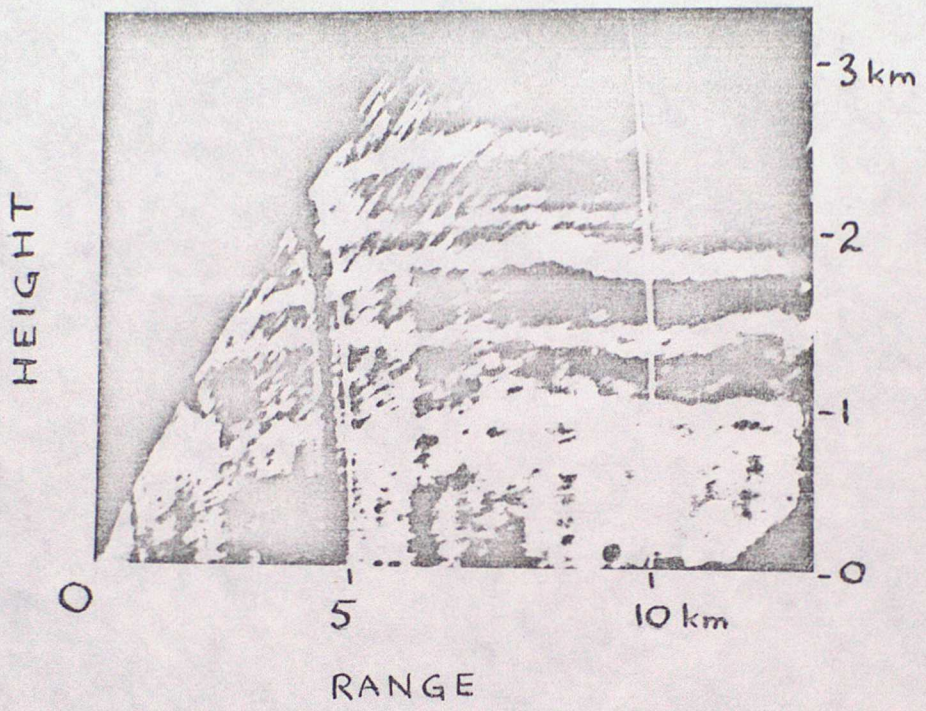

Fig 23a

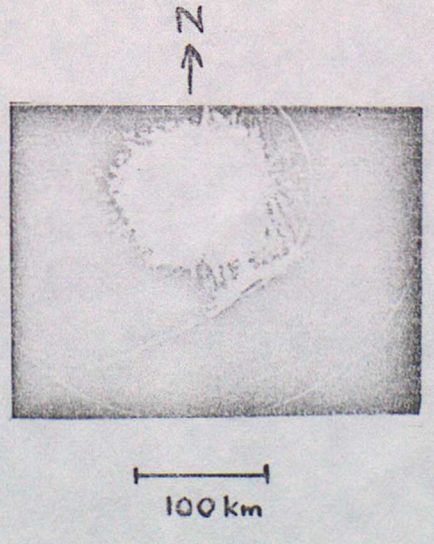

Fig 23b

Fig 22

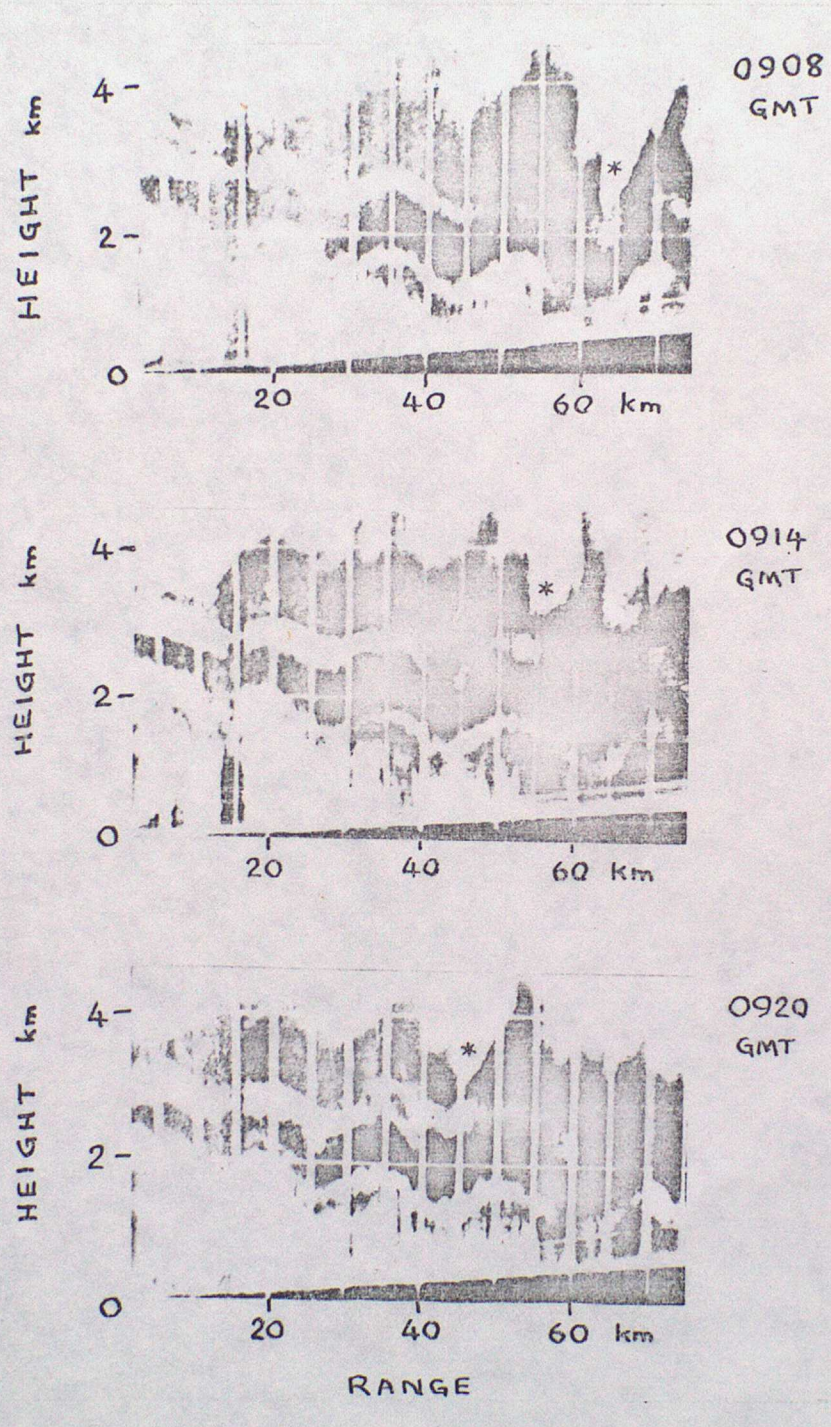
0908
GMT
HEIGHT km
4
2
0
20
40
60 km
0914
GMT
HEIGHT km
4
2
0
20
40
60 km
0920
GMT
HEIGHT km
4
2
0
20
40
60 km
RANGE

Fig 24

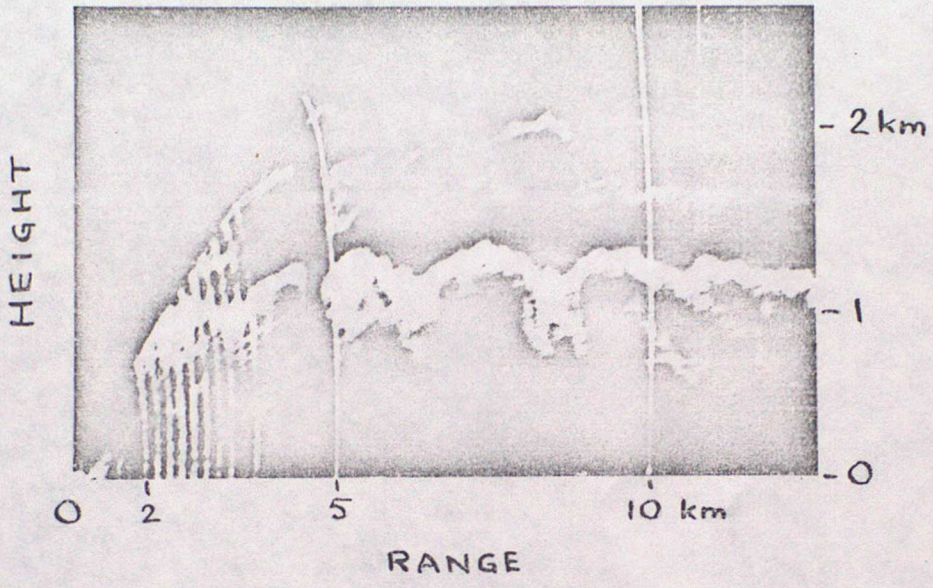

Fig. 25

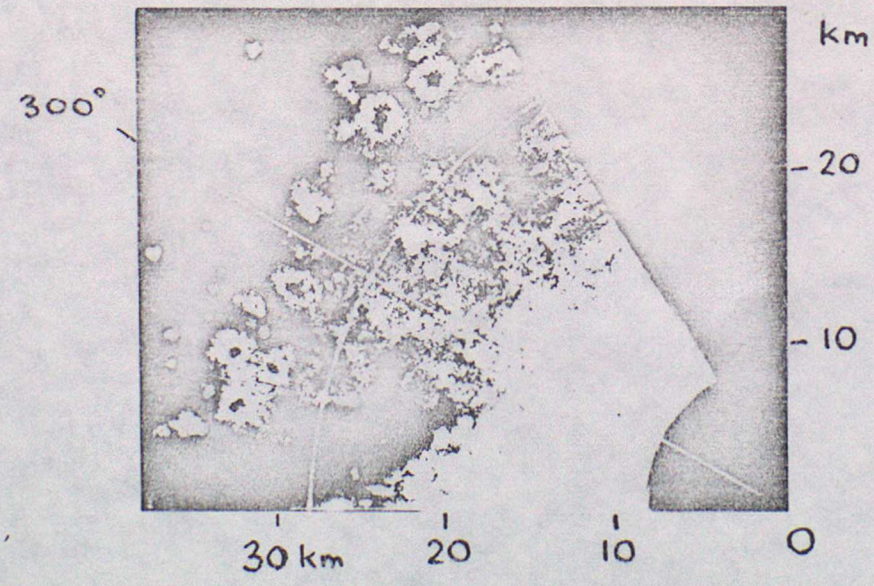

Fig 26

(a) (b)

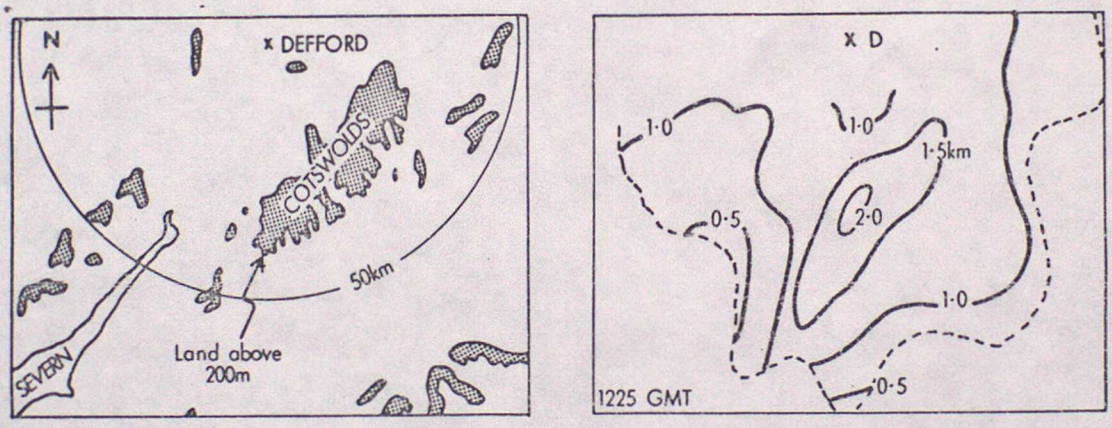
N
x DEFFORD
COTSWOLDS
50km
Land above
200m
SEVERN
X D
1·0
1·0
1·5km
0·5
2·0
1·0
0·5
1225 GMT

Fig 27

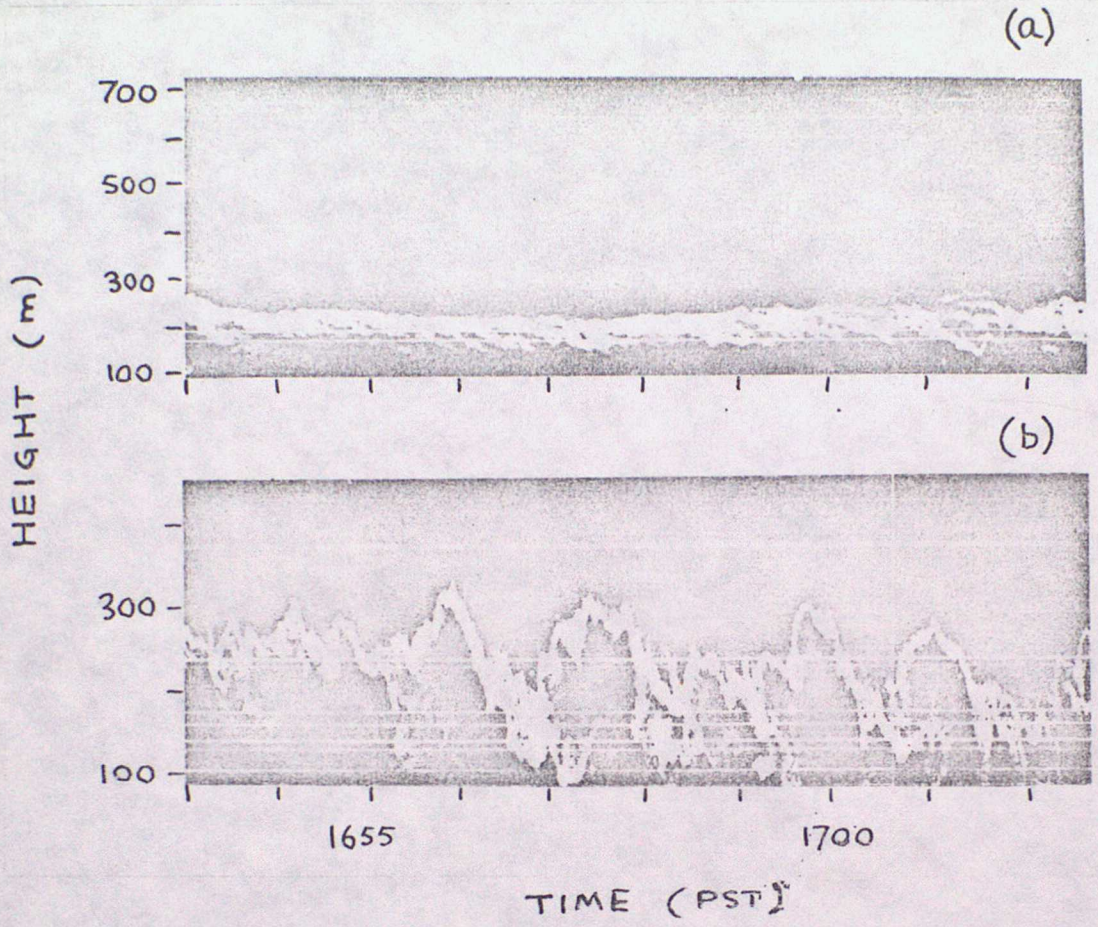
(a)
700
500
300
100
(b)
300
100
HEIGHT (m)
1655
1700
TIME (PST)

Fig 28

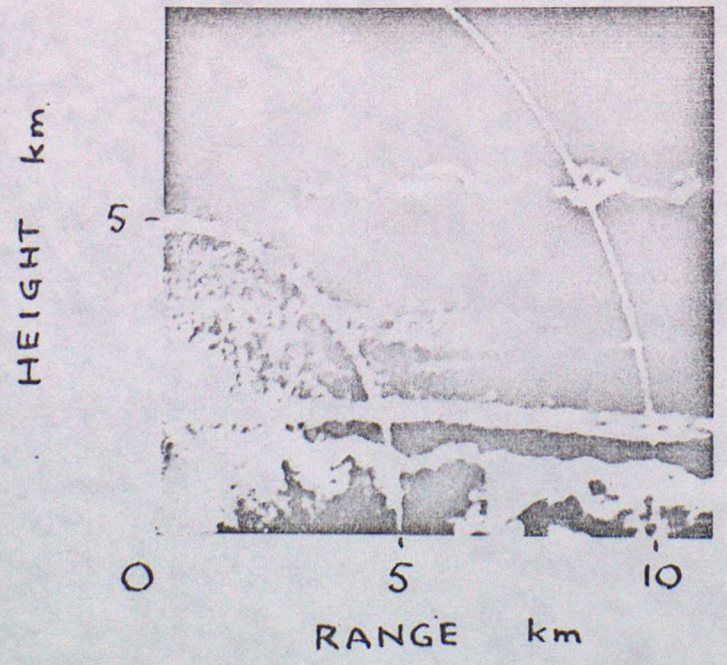
HEIGHT km
5
0
5
10
RANGE km

METEOROLOGICAL OFFICE RADAR RESEARCH LABORATORY - MET.O. RRL.

Research Reports.

No.1. The Short Period Weather Forecasting Pilot Project.
(MRCP 426) K A Browning.

No.2. Observation of Strong Wind Shear using Pulse Compression Radar.
K A Browning. P K James (Met.O. RRL). D M Parkes. C Rowley.
A J Whyman (RSRE).

No.3. Assessment of a Real-Time Method for Reducing the Errors in Radar Rainfall Measurements due to Bright-Band.
J L Clarke, RSRE. C G Collier, Met.O. RRL.